Engineering 54 (2025) 320–345

Contents lists available at ScienceDirect

Engineering

journal homepage: www.elsevier.com/locate/eng

Research
Civil Engineering—Article

# Resilience Models for Tunnel Recovery After Earthquakes

Zhong-Kai Huang [a], Nian-Chen Zeng [a], Dong-Mei Zhang [a,b,*], Sotirios Argyroudis [c,e,*], Stergios-Aristoteles Mitoulis [d,e]

[a] Department of Geotechnical Engineering, Tongji University, Shanghai 200092, China
[b] State Key Laboratory of Disaster Reduction in Civil Engineering, Tongji University, Shanghai 200092, China
[c] Department of Civil and Environmental Engineering, Brunel University of London, Uxbridge UB8 3PH, UK
[d] The Bartlett School of Sustainable Construction, University College London, London WC1E 7HB, UK
[e] MetaInfrastructure.org, London NW11 7HQ, UK

ARTICLE INFO

*Article history:*
Received 13 September 2024
Revised 5 May 2025
Accepted 23 June 2025
Available online 27 June 2025

*Keywords:*
Tunnel
Resilience assessment
Expert opinion survey
Restoration model
Functionality loss

ABSTRACT

Tunnels are a crucial component of urban infrastructure, continuously exposed to various hazards, threats, and stressors. Events such as earthquakes, fires, and floods, along with aging and construction-related disturbances, pose significant challenges to tunnel resilience. Reliable fragility, restoration, and traffic reinstatement models are essential for assessing and quantifying resilience, as they allow infrastructure operators to prioritize maintenance and adapt to evolving threats in complex transportation systems. Although the vulnerability and fragility of tunnels have been widely researched over the last decade, studies focusing on tunnel restoration to quantify resilience remain scarce. This gap prevents operators from implementing proactive and reactive adaptation measures to ensure seamless tunnel functionality. To address this issue, this study presents a novel, fit-for-purpose, damage-level-dependent probabilistic approach for quantifying tunnel recovery. It introduces the first realistic, practice-led restoration models that enable resilience quantification in tunnels. To develop these models, a global expert survey was conducted to establish reinstatement (traffic capacity) and restoration (structural capacity) models tailored to tunnel resilience assessments. A detailed questionnaire was designed to gather expert input on required restoration tasks, their duration, sequencing, and cost. The survey focused primarily on damage induced by seismic events, incorporating idle times and traffic capacity gains over time. The results were then used to generate deterministic and probabilistic reinstatement and restoration models. The deterministic models are intended for practical applications, while the probabilistic models account for epistemic uncertainties and are presented in a reproducible format for further development across different hazards and applications. A case study is included to demonstrate the resilience assessment of a typical tunnel using the newly developed restoration models. The findings will help infrastructure operators and city planners to accurately assess tunnel resilience, enabling informed investment decisions.



## 1. Introduction

With the rapid expansion of underground spaces, tunnels have become an integral part of urban infrastructure [1–5]. The ability of tunnels to operate normally after natural or human-caused disasters such as earthquakes, landslides, floods, or explosions is of great concern for infrastructure owners, stakeholders, and the wider community. Studies have demonstrated that critical infrastructure exposure to multiple hazards can result in severe structural damage and significant socio-economic losses [6–9]. For instance, on February 6, 2023, a magnitude-7.8 earthquake hit southeastern Türkiye, causing over 5000 fatalities and widespread damage to infrastructure, including tunnels and residential buildings [10–12]. Similarly, during the Chi-Chi earthquake in Taiwan of China, approximately 49 tunnels within a 60 km radius of the epicenter suffered structural damage, including steel reinforcement deformation, displaced linings, portal failure, spalling, and concrete cracking [13,14]. After the 2016 Norcia earthquake in Italy, large vertical cracks were found on the southern sidewall of the San Benedetto Tunnel [15]. A train loaded with hazardous

* Corresponding authors.
*E-mail addresses:* dmzhang@tongji.edu.cn (D.-M. Zhang), sotirios.argyroudis@brunel.ac.uk (S. Argyroudis).

https://doi.org/10.1016/j.eng.2025.06.028

materials derailed and exploded in the Howard Street Tunnel in Baltimore, USA. The explosion caused a massive fire that burned for several days, severely damaging the tunnel and disrupting traffic [16]. Another case was the Daegu Metro fire (2003) in Republic of Korea, which caused 198 deaths and 146 injuries [17,18]. The cover arch at the exit of the Wenling Tunnel, a single tunnel in Daying–Shenchi Expressway, in China was broken and cracked after a landslide [19]. Hurricane Sandy flooded seven subway tunnels and three vehicle tunnels in New York City in 2012, disrupting traffic for several days [20]. Recently, due to an extreme rainstorm, flooding occurred on Metro Line 5 in the capital city of Zhengzhou, Henan Province, China, tragically causing 14 fatalities [21]. Additionally, a collision between a tanker carrying liquefied petroleum gas and a coach led to an explosion inside a tunnel along the Palermo–Punta Raisi motorway (Italy). This accident caused five fatalities, 32 injuries, and severe damage to the tunnel structures [22]. These real-life cases underscore the vulnerability of tunnels to extreme natural and human-induced hazards that can lead to significant losses in traffic and structural capacity, disrupting transportation networks.

To maintain the integrity, continuity, and functionality of infrastructure assets and networks during extreme events and to align with the United Nations Sustainable Development Goals (SDGs) [23], infrastructure owners and operators must urgently develop and implement measures to improve resilience before and after extreme disasters [24–26]. Resilience, a rapidly developing concept in lifeline engineering, refers to the ability to withstand, respond to, and recover quickly from a disruptive or catastrophic event [27–30]. It encompasses four main properties: robustness, rapidity, redundancy, and resourcefulness [31,32]. Robustness reflects the inherent ability of infrastructure to resist the impact of extreme events and can be improved through advanced design and construction methods [33–35]. Rapidity is defined as the ability to quickly recover the functionality or structural capacity of an infrastructure to its pre-disaster state and is closely related to post-disaster recovery strategies [33–35]. Redundancy ensures the replaceability of system components to maintain system functionality in the event of a disruption [34–36]. Resourcefulness represents the ability to make timely decisions and rationally mobilize the required resources in response to emergencies [36,37].

The quantification of infrastructure resilience is based on the resilience curve which describes the robustness of a structure and the speed of its functional recovery after an event. Fragility is commonly quantified using fragility curves that express the probability of damage as a function of the intensity measure (IM) [38]. Numerous studies have been conducted to determine the fragility functions of critical assets to extreme natural events using empirical, analytical, expert elicitation, and hybrid approaches [39–47]. Vulnerability is characterized by the susceptibility of a structure or system to damage at a specific hazard level and is often represented by fragility functions [48]. Seismic vulnerability assessment of tunnels is a topic of great interest in the field of underground engineering. Understanding tunnel failure mechanisms under seismic action is critical for developing robust fragility functions. Extensive deterministic analyses have been conducted to investigate the seismic behavior of tunnels, including numerical studies [49–53], analytical studies [54–57], experimental studies [58–60], and monitoring studies [61,62]. The derivation of fragility functions has driven a large body of research into the quantitative assessment of the resilience of tunnels subjected to seismic actions [63–65].

To quantify restoration speed, predict recovery paths, and estimate recovery time, it is crucial to establish adequate restoration models [66–68]. Several post-disaster restoration models have been developed, especially for critical urban assets such as hospitals [68,69], residential buildings [70], and bridges [71–73], to assess the resilience of cities under extreme disasters. They are usually presented in different forms such as linear [74], trigonometric [75], stepwise [76], and continuous [74]. However, to the best of the authors' knowledge, restoration models for tunnels exposed to seismic hazards are limited and primarily rely on simple mathematical modeling and the Federal Emergency Management Agency (FEMA) methodology [77], which is based on the input provided by Applied Technology Council-13 (ATC-13) report published in 1985. Consequently, it has not been updated with recent advances in resilience engineering. Furthermore, current empirical restoration models fail to represent the underlying restoration logic, as they do not account for required restoration tasks, their duration, sequence, and idle time. Given the significant uncertainty inherent in the repair process, restoration models based on deterministic approaches cannot capture potential evolutionary trends and dynamic variations in repair pathways. The lack of rigorous post-hazard tunnel restoration models that quantify the uncertainties associated with the recovery process prevents us from modeling the recovery process, estimating the loss of traffic capacity, and conducting accurate resilience assessments for asset management and adaptation.

To fill these gaps, a comprehensive questionnaire was developed to gather information from experienced experts. The survey included definitions of damage levels, restoration tasks and their prioritizations, reinstatement of traffic capacity, idle time, and cost ratio (i.e., repair cost relative to replacement cost). By identifying and quantifying the key parameters in the repair process, deterministic and probabilistic resilience models for tunnels were established based on a damage-level-dependent approach. These models are more rigorous and better reflect the real repair processes than previous empirical restoration models. This methodology is replicable and applicable to other critical assets affected by various types of disasters. The restoration models help quantify resilience and optimize the repair process for tunnels with various levels of damage. In addition, they inform resource mobilization strategies, facilitate resilience-based management, and reduce traffic disruptions.

## 2. Expert-elicited restoration strategies for tunnel resilience

The framework for assessing the resilience of tunnels to natural or human-induced disasters, and how expert-elicited restoration strategies play a key role in quantifying resilience is shown in Fig. 1. This methodology is not limited to tunnels but applies to a wide range of critical infrastructures exposed to natural disasters. The framework consists of five main steps. The first step (Step 1) involves hazard characterization, with an emphasis on individual natural hazards such as earthquakes and floods. Each hazard is described by an IM, which quantifies the extent of the disaster's impact on the structure or system and is usually related to structural damage or system disruption. For example, in the case of floods, IM could be the flow depth, water discharge, and scour depth [33,34,78]. In earthquake disasters, peak ground acceleration (PGA) and peak ground velocity (PGV) are often used to characterize the intensity of seismic hazards [63,64]. Additionally, defining structural or systemic damage levels is essential, as they depend on damage mechanisms, structural design requirements, and stakeholder considerations. The second step (Step 2) is vulnerability assessment, which is based on realistic fragility functions. These functions can be generated based on numerical simulations, empirical data, or expert judgement [39–47]. Fragility curves help determine the probability of an infrastructure asset being in a damage state (DS) at a given hazard intensity. The third step (Step 3) is the assessment of damage recovery, which includes many

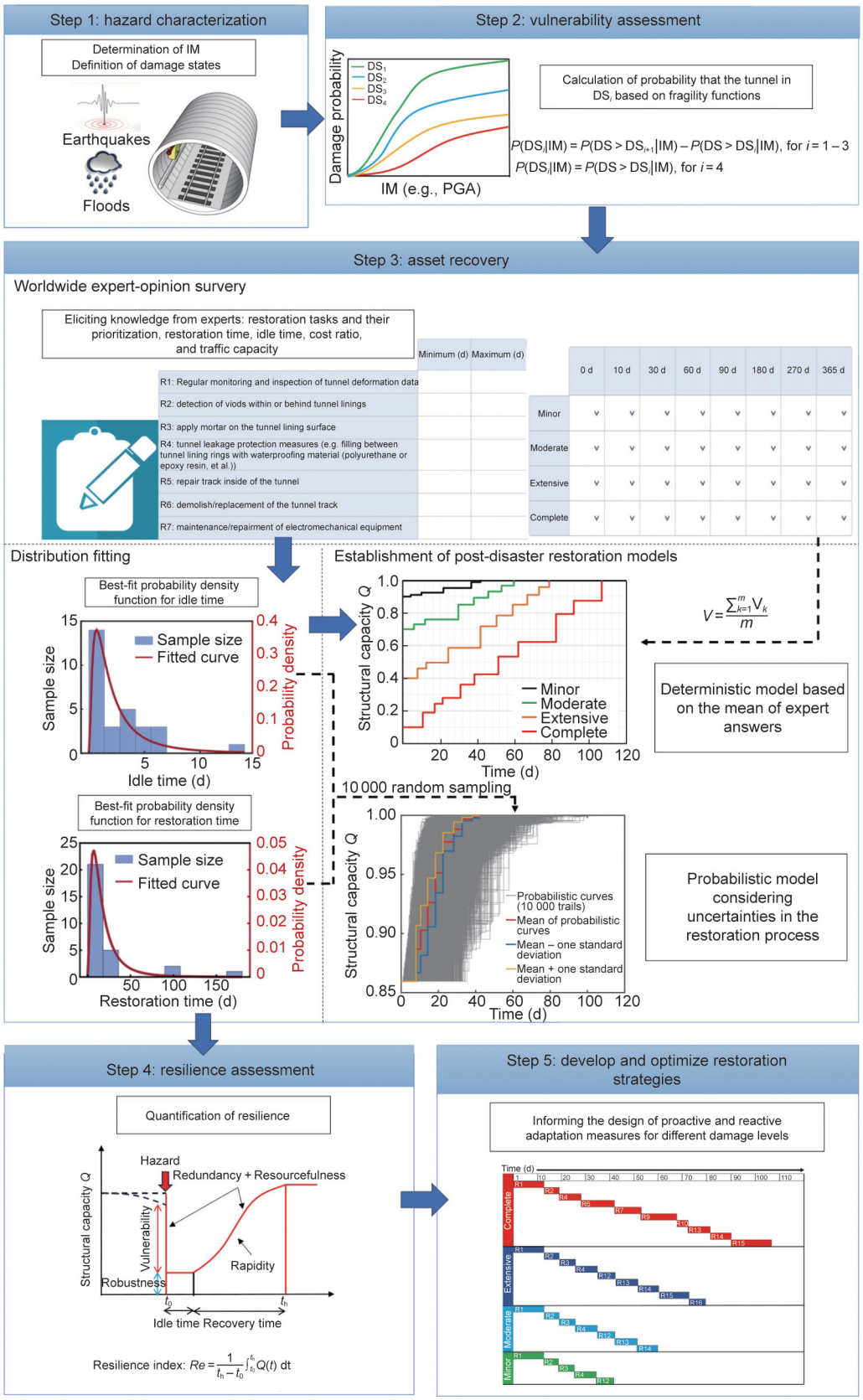


**Fig. 1.** Resilience assessment framework for tunnels exposed to hazard. $DS_i$: a specific damage state (DS), where $DS_1$, $DS_2$, $DS_3$, and $DS_4$ represents the minor, moderate, extensive, and complete DSs, respectively; $P(DS_i|IM)$: probability of the tunnel being in $DS_i$ at a given seismic intensity; $P(DS > DS_i|IM)$: probability of the damage exceeding a $DS_i$; $V$: the mean value of the key random variable for the entire post-hazard restoration process; $V_k$: discrete sample $k$ collected through the questionnaire; $m$: number of valid samples; $Re$: resilience index; $t_h$: control time; $t_0$: time of the hazard occurrence; $Q(t)$: structural capacity at time $t$.

uncertainties, such as the duration of restoration tasks, sequence of repair tasks, and idle time. To obtain these key variables in the repair process, a worldwide expert opinion survey was conducted. Based on expert knowledge from the survey, deterministic and probabilistic restoration models (structural capacity) and reinstatement models (traffic capacity) were established. The deterministic model was based on mean values of these variables. Considering cognitive uncertainty, the distribution of the variables was fitted, and probabilistic models were then formed by random sampling. Finally, by combining the identified hazards and IMs (Step 1), fragility functions determined in Step 2, and restoration models established in Step 3, resilience curves were generated, and resilience indices were calculated. To achieve the rapid restoration of tunnel functionality with limited resources, post-disaster restoration strategies were developed and optimized. These strategies include selecting rehabilitation tasks and determining optimal rehabilitation sequences.

Rational restoration models are indispensable components of resilience evaluation frameworks. To establish deterministic and probabilistic restoration models, uncertainties such as the duration of restoration tasks, idle time, and cost ratio must be quantified throughout the restoration process. Conducting a comprehensive survey provides a reliable method for obtaining these uncertainties by directly eliciting knowledge from experts in tunnel rehabilitation. Therefore, a detailed questionnaire was prepared for typical circular tunnels that have sustained varying levels of damage from threats such as earthquakes. This questionnaire was designed to support the development of restoration and reinstatement models. It incorporated definitions of damage levels, duration and priority of restoration tasks, cost ratio, and traffic capacity throughout the entire restoration process. Before completing the questionnaire, experts were asked to rate their expertise in tunnel rehabilitation, which helped assess the reliability of the research results. The survey on tunnel damage restoration was divided into four sections: ① instructions, ② restoration tasks, ③ description of a typical tunnel, and ④ parameters for quantifying tunnel restoration. Experts could also provide additional comments on the survey format, their professional experience in tunnel rehabilitation, damage levels, tunnel traffic capacity, repair procedures, or any other relevant factors they considered important or insufficient.

### 2.1. Benchmark tunnel and damage level

Considering that tunnel performance and restoration models are highly dependent on specific design objectives, a typical circular metro tunnel, commonly found in modern underground systems, was selected as the benchmark tunnel for the questionnaire. This selection was made to enhance the applicability of resilience models. This study focused on the damage restoration tasks of ten segmental prefabricated tunnel liners, each with a longitudinal length ($L$) of 12 m, as shown in Fig. 2. The outer diameter ($D$) was 6.2 m, and the lining thickness ($h$) was 0.35 m. The burial depth (i.e., the distance from the ground surface to the tunnel crown) was approximately 10 m. A cross-section of the assembled segmental lining ring is shown in Fig. 2(a). Each integrated lining ring comprises six precast concrete segments: one key segment (F), two adjacent segments (L1 and L2), two standard segments (B1 and B2), and one bottom segment (B). These segments were linked using radial joints with two steel bolts. When the metro tunnel was put into operation, the segment at the bottom was covered by a track bed to support the track rail. Generally, a steel track rail and a cast-in-place C35 concrete track bed are adopted for metro tunnels [79]. The benchmark tunnel represents a standard design that encapsulates the essential features of segmental-lining tunnels prevalent in soft-ground tunneling. In addition, its configuration is well documented in the literature, and numerous case studies and empirical data are available. This allows for more robust analysis and validation of restoration models [46,80,81]. It is assumed that the tunnel is of average importance, meaning no additional resources are allocated to the tunnel after a hazard occurs.

Before the expert provides feedback on the restoration of the tunnel, damage levels (i.e., minor, moderate, extensive, and complete) must be defined in the questionnaire. The selection of appropriate indicators to classify the extent of damage is crucial as these will have a direct influence on the repair strategy. Convergence is widely accepted in literature as an important performance indicator for tunnels [82–84], as it reflects both serviceability and safety during operation. It is also easily obtained through on-site monitoring. Additionally, several national and regional design codes limit normalized convergence or the convergence ratio $\Delta D/D$ (where $\Delta D$ denote the horizontal convergence of a shield tunnel). For example, the British tunnel standard "Tunnel Lining Design Guide" [85] limits the normalization convergence to 2%, while the Chinese code [86] for rail transit system sets the $\Delta D/D$ as the serviceability criteria at 3‰–5‰. Therefore, the convergence ratio serves as one of the quantitative indices for defining damage levels. In addition to the deformation index, the index of the structural internal force, which is the ratio of the actual tunnel cross-sectional bending moment ($M$) to its moment bearing capacity ($M_{Rd}$), is also used to classify damage levels. This damage index, first proposed by

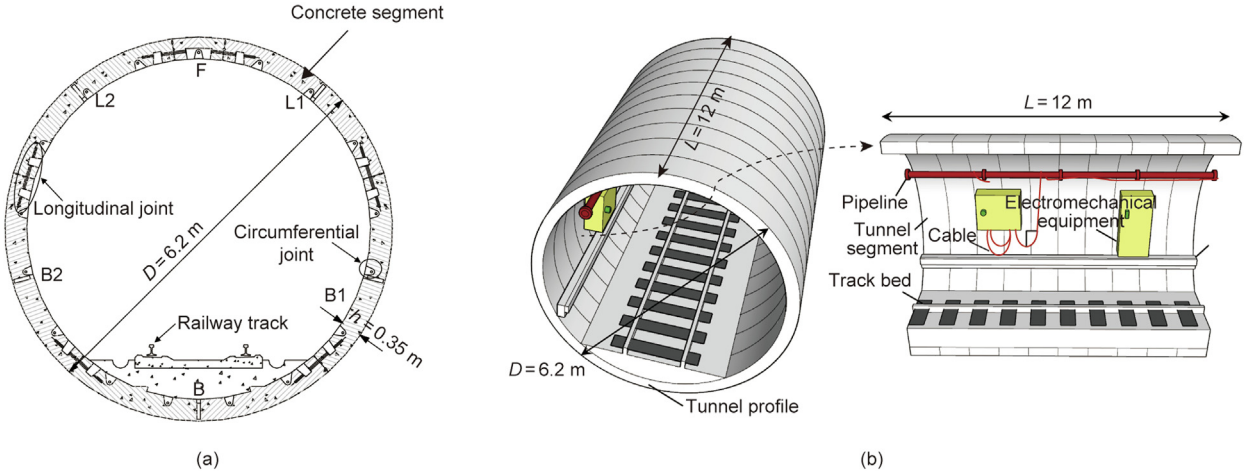


**Fig. 2.** Schematic of the benchmark tunnel. (a) Typical cross section of the assembled segmental lining ring. (b) Examined 10 segment tunnel lining with a length of 12 m in the longitudinal direction.

Argyroudis and Pitilakis [87], has been widely used in research on the seismic vulnerability of tunnels [88–91]. Extensive statistical studies on the damage characteristics of tunnel structures under seismic hazards have also led to the inclusion of additional criteria in damage level classification. These include crack width in tunnel liners, inverted uplift, and dislocation of track rails [14,92,93]. The detailed classification criteria and threshold values for the damage levels of tunnels are listed in Table 1 [14,92,93].

### 2.2. Restoration model development based on expert elicitation

To develop representative and efficient restoration models for tunnels, it is crucial to understand and optimize the entire restoration process for tunnels with various levels of damage. Restoration tasks and their prioritization, idle time, post-damage traffic capacity, and cost ratio for each damage level are crucial factors that must be closely monitored throughout the restoration process. Consequently, experts were asked to provide comprehensive estimates of these factors based on their professional judgment and actual data from previous case studies.

#### 2.2.1. Restoration tasks

The questionnaire presents 20 post-hazard restoration tasks (R1–R20) for damaged tunnels, including both structural and non-structural interventions. The numbering of these tasks does not necessarily indicate their sequence. The restoration tasks and their appropriate order for tunnels at different damage levels were provided by the experts. Additionally, experts were expected to suggest supplementary restoration tasks based on their knowledge and professional experience. Such tasks may include strength testing of lining samples and inspections of reinforcement conditions and deterioration. After identifying and prioritizing potential restoration tasks, experts were asked to provide an estimate of the maximum and minimum durations for each task, as shown in Table S1 in Appendix A.

Table 2 categorizes the 20 restoration tasks according to intervention type. These tasks were grouped into four main categories:

**Table 1**
Definition of damage levels of the examined tunnel section [14,92,93].

| Damage level | Description | Sketch (not in scale) |
|---|---|---|
| Minor | The ratio of the actual tunnel cross-sectional bending moment ($M$) to the moment bearing capacity ($M_{Rd}$) $M/M_{Rd}$: 1–1.5<br>Tunnel convergence ratio $\Delta D/D$ : 0.6‰–2.5‰<br>Cracking width of tunnel liners: 0–3 mm<br>Invert uplift: < 10 cm<br>Dislocation of the track rail: < 10 cm<br>Electromechanical equipment is slightly damaged | 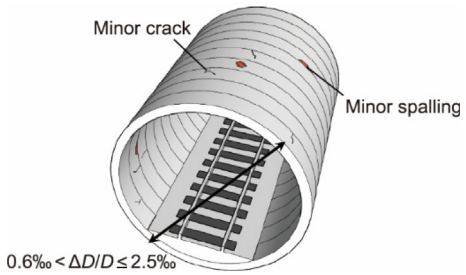 |
| Moderate | $M/M_{Rd}$: 1.5–2.5<br>$\Delta D/D$ : 2.5‰–4.0‰<br>Cracking width of tunnel liners: 3–35 mm<br>Invert uplift: 10–20 cm<br>Dislocation of the track rail: 10–20 cm<br>Electromechanical equipment is moderately damaged | 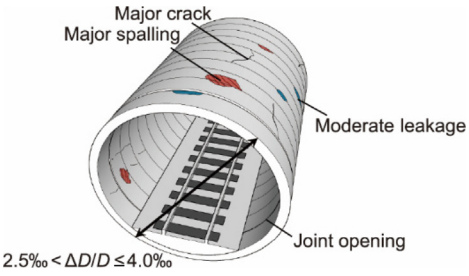 |
| Extensive | $M/M_{Rd}$: 2.5–3.5<br>$\Delta D/D$ : 4.0‰–6.0‰<br>Cracking width of tunnel liners: > 35 mm<br>Invert uplift: > 20 cm<br>Dislocation of the track rail: > 20 cm<br>Electromechanical equipment is extensively damaged and remains partially operational | 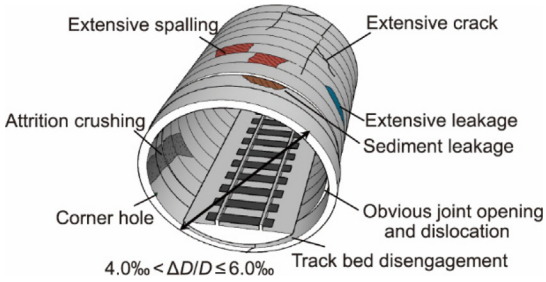 |
| Complete | $M/M_{Rd}$: > 3.5<br>$\Delta D/D$ : > 6.0‰<br>Collapse of the liner or surrounding soils to the extent that the tunnel is blocked either immediately or with a few days after the main shock<br>Complete damage of tunnel track; extensive dislocation of the track rails<br>Electromechanical equipment is non-operational | 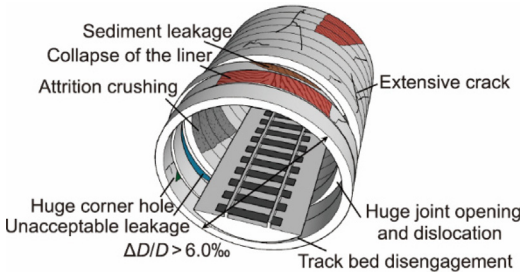 |

**Table 2**
Types of diverse restoration tasks.

| Category | Restoration tasks |
|---|---|
| Reinforcement of lining structures | R3, R4, R10, R11, R12, R13, R14, R15, R16, R17, R18, and R20 |
| Repair/replacement of installations and utilities | R5, R6, and R7 |
| Ground improvement | R8, R9, and R19 |
| On-site monitoring | R1 and R2 |

reinforcement of lining structures, repair/replacement of installations and utilities, ground improvement, and on-site monitoring. Most restoration tasks, such as the installation of steel plates on the inner surface of lining rings, can be categorized as maintenance and reinforcement of lining structures, which is one of the most frequently required actions. The tasks listed in Table 2 are common tasks for typical circular tunnels and do not include specialized tasks, such as cover-arch reinforcement methods, which are typically employed for strengthening and supporting tunnels that have water leakage problems [94–98].

*2.2.2. Idle time*

Idle time is the interval between the occurrence of damage to tunnels due to extreme events and the initiation of restoration work. This time may include, but is not limited to, emergency response, inspection and condition assessment, site investigation, structural evaluation, and the design of mitigation measures. For this study, idle time was factored into the resilience assessment because of its impact on the overall speed of the restoration process. Experts were asked to provide rough estimates for minimum and maximum idle times, as shown in Table S2 in Appendix A.

*2.2.3. Cost ratio*

The cost ratio is an estimate of the cost of restoring a damaged tunnel to normal operation relative to the total construction cost of all structural components. For example, a repair cost ratio equal to 0.15 means that the cost of restoration is equal to 15% of the cost of reconstruction. In practical terms, if the tunnel costs $3.0 \times 10^6$ USD, the cost of restoration would be estimated at $4.5 \times 10^5$ USD (tunnel costs × 0.15). The experts provided rough estimates of the cost ratio (percentage of the tunnel replacement cost) depending on the damage level, as shown in Table S3 in Appendix A. These estimates could be single values (e.g., 0.15) or expressed as a range (e.g., 0.10–0.15).

*2.2.4. Traffic capacity of tunnel*

The expected traffic capacity of the tunnel after the damage (in percent (%)) is the measure for the "traffic restriction" of the tunnel for each damage level and for each point in time after the commencement of restoration works. The questionnaire defined three levels of tunnel traffic capacity: 100% (fully operational), 50% (reduced traffic), and 0 (not operational/closed), corresponding to the full functionality state, partial functionality state, and zero functionality, respectively. A transportation capacity of 50% means that the daily train frequency and/or speed has been reduced to reflect an overall 50% reduction in service compared with normal operation (fully functional) [99]. The experts were asked to estimate the expected traffic capacity of the tunnel at eight specific time points (0, 10, 30, 60, 90, 180, 270, and 365 d after the commencement of restoration work) for each damage level, as shown in Table S4 in Appendix A. Of these, 10 d is a critical time point for the post-earthquake emergency period [100], while the remaining seven time points correspond to representative phases, such as one month, six months, and one year after the commencement of restoration work. These intervals were selected to simplify the questionnaire and ensure that all the experts responded using a consistent timescale.

*2.2.5. Restoration task prioritization*

Selecting and prioritizing appropriate restoration tasks for varying damage levels is key to establishing both deterministic and probabilistic restoration models [34]. Experts were asked to select the restoration tasks that should be applied to restore the normal operation of the damaged tunnel and to propose a logical sequence for implementing these restoration tasks, as shown in Table S5 in Appendix A.

*2.3. Geographical distribution and professional experience of experts*

To obtain diverse perspectives on resilience models worldwide, the questionnaire was distributed online from December 17, 2023 to January 15, 2024. In total, more than 200 experts were contacted, and 33 ultimately provided feedback. The experts came from the fields of underground and infrastructure engineering, geotechnics, and earthquake engineering. They come from renowned consulting offices and universities and have a wealth of theoretical knowledge and practical experience in the fields of tunnel design, construction, inspection, maintenance, and reinforcement. Most of the experts have more than 10 years of professional experience, which enhanced the reliability of the survey results. To mitigate regional biases stemming from differences in design culture and construction standards in different regions and countries, the survey participants were selected from different geographical locations. Experts from 13 countries contributed data, providing a global perspective on tunnel resilience models. This international collaboration minimizes regional bias and improves the generalizability of the findings. The geographical distribution of the experts by country and region is shown in Fig. 3.

## 3. Results and discussion

This section presents the results from the analysis of tunnels exposed to seismic hazards. For ease of application, both deterministic and probabilistic restoration models were developed based on expert responses from 33 completed questionnaires from academics, consultants, and scientists from research institutions. The deterministic restoration models are derived from the experts' answers, which capture the representative core information from

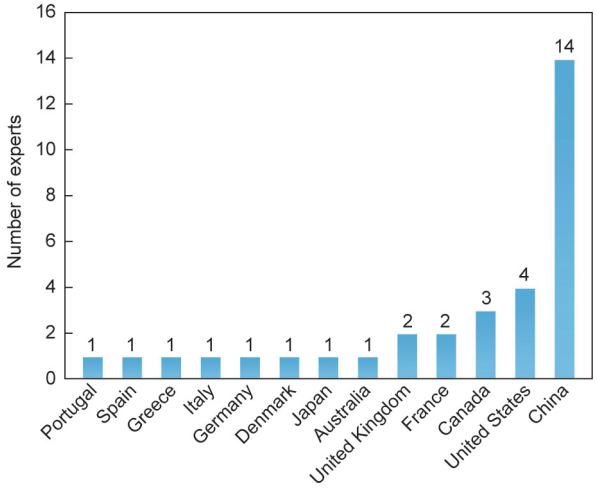


**Fig. 3.** Geographical distribution of experts by country and region.

substantial amounts of data and facilitate the identification of key trends in the post-disaster functional evolution of damaged tunnels. The effectiveness of various restoration tasks under different damage levels can be assessed using deterministic restoration models, thereby enabling scientifically informed repair strategies. To account for cognitive biases and inherent uncertainties in the restoration process, a distribution fitting analysis was performed on the survey results, including idle time, restoration time, and cost ratio. The optimally fitted distributions accurately identify the distribution range, central tendency, and dispersion of the random variables. Subsequently, probabilistic restoration models were established by performing random samplings within the optimally fitted distributions. Probabilistic restoration models are crucial for assessing the reliability of repair strategies because they consider unpredictability in practical engineering. By incorporating uncertainty into the analysis, potential variations in repair outcomes can be better predicted and more adaptable and flexible restoration strategies can be developed.

### 3.1. Restoration tasks

#### 3.1.1. Deterministic models of restoration time

To visualize the expert responses collected from the questionnaire on the duration of 20 post-hazard repair tasks, this section begins with a statistical analysis of discrete samples. The analysis primarily involves the use of Eq. (1), to determine the mean values of the minimum and maximum durations for each restoration task. These mean values can be readily applied to quantitative restoration time estimations, thereby facilitating the development of deterministic restoration time models.

$$V = \frac{\sum_{k=1}^{m} V_k}{m} \tag{1}$$

where $V$ represents the mean value of the key random variable for the entire post-hazard restoration process, such as the duration of the restoration tasks, idle time, and cost ratio; $V_k$ represents the discrete sample $k$ collected through the questionnaire; $m$ is the number of valid samples.

Table 3 presents statistical results derived from expert responses, including the duration of each restoration task. The second and third columns of Table 3 display the mean values of the minimum and maximum restoration times, respectively, for each task. The fourth column shows the mean values of the second and third columns.

It is evident that the more time-consuming restoration tasks typically involve replacing tunnel structural components (e.g., replacing tunnel tracks and connecting bolts of tunnel segments) or reinforcing tunnel structures and soil (e.g., applying fiber-reinforced plastics (FRP) to the inner surface of the lining and soil improvement through grouting). In contrast, monitoring tasks are less time consuming but require frequent execution [97].

#### 3.1.2. Probabilistic models of restoration time

The maximum and minimum restoration times for tasks R1–R20 given by experts based on their specialized knowledge and practical engineering experience are often subject to cognitive uncertainty.

To account for this variability, probabilistic recovery time models were developed based on the collected discrete samples. Specifically, ten intervals were evenly divided between 0 and the maximum values in the collected dataset. For example, 30 d was the maximum value among the 33 collected samples for the R1 minimum restoration time, so the minimum restoration time for R1 was divided into ten consecutive intervals from 0 to 30 d. The sample size in each interval was determined to construct corresponding histograms. Based on this analysis, empirical probabilistic distribution functions were developed, including normal, lognormal, exponential, generalized extreme value (GEV), and Gamma. This approach is a widely employed statistical method that accurately describes the behavior of random variables based on observed data, effectively characterizing their variability and uncertainty [101–103]. The optimal fit was then determined by comparing the mean squared error (MSE) and $R$-squared ($R^2$, coefficient of determination), which are commonly used indicators to assess the fitting performance in probabilistic analyses [104,105]. The corresponding probability density functions and their key parameters are presented in Table S6 in Appendix A. Figs. 4 and 5 show the histograms of the minimum and maximum restoration times for the 20 restoration tasks, respectively, along with the best-fit probability density functions plotted in each histogram. Additionally, Tables 4 and 5 present the best-fit distributions for the minimum and maximum restoration times for each restoration task, respectively, along with their numerical characteristics and key parameters. It was observed that the minimum restoration

**Table 3**
Minimum, maximum, and mean values of restoration time per damage level for each restoration task.

| Restoration task | Duration (d) | | |
|---|---|---|---|
| | Minimum | Maximum | Mean |
| R1: regular monitoring and inspection of tunnel deformation data | 5.02 | 20.35 | 12.69 |
| R2: detection of voids within or behind tunnel linings | 3.13 | 9.14 | 6.14 |
| R3: apply mortar on the tunnel lining surface | 3.61 | 9.57 | 6.59 |
| R4: tunnel leakage protection measures (e.g., filling gaps between tunnel lining rings with waterproofing materials such as polyurethane or epoxy resin) | 4.58 | 13.52 | 9.05 |
| R5: repair track inside of the tunnel | 4.30 | 14.69 | 9.50 |
| R6: demolish/replacement of the tunnel track | 6.53 | 21.00 | 13.77 |
| R7: maintenance/repairment of electromechanical equipment | 4.59 | 17.61 | 11.10 |
| R8: use grouting for the soil improvement from inside of the tunnel lining | 5.63 | 19.59 | 12.61 |
| R9: use grouting from ground surface for the soil improvement at the two sides of the tunnel spring line | 7.17 | 22.54 | 14.85 |
| R10: removal of debris inside of the tunnel | 2.47 | 6.69 | 4.58 |
| R11: tunnel rebar erosion protection measures | 5.69 | 18.75 | 12.22 |
| R12: repair tunnel lining cracks | 3.84 | 10.60 | 7.22 |
| R13: repair tunnel lining spalling with concrete | 5.06 | 13.33 | 9.20 |
| R14: replacement of connecting bolts of tunnel segment | 4.55 | 12.59 | 8.57 |
| R15: temporary support of the tunnel lining | 6.23 | 18.21 | 12.22 |
| R16: apply fiber-reinforced plastics (FRP) to the inner surface of lining locally | 3.55 | 10.03 | 6.79 |
| R17: insert steel plates to adhere to the inner surface of lining along the local or full ring | 5.39 | 13.93 | 9.66 |
| R18: add reinforced concrete secondary lining | 9.84 | 23.53 | 16.69 |
| R19: conduct artificial freezing of regional strata | 11.70 | 35.10 | 23.40 |
| R20: reconstruction/replacement of the tunnel | 39.48 | 97.36 | 68.42 |

time for most restoration tasks obeyed a lognormal (R1, R2, R3, R4, R14, R15), Gamma (R5, R6, R8, R9, R13, R18, R20), or exponential distribution (R7, R11, R12, R16, R17, R19). Only the minimum restoration time of R10 obeyed a GEV distribution. In terms of the maximum restoration time, the lognormal function best fits most restoration tasks, whereas the exponential function best fits R2 and R18, the GEV function best fits R10, R12, and R16, and the Gamma function best fits R11, R17, and R20.

### 3.2. Idle time

#### 3.2.1. Deterministic models of idle time

Idle time is a key variable in post-hazard restoration, significantly influencing the speed of the restoration process. Taking timely measures following an extreme hazard can prevent further deterioration of the lining structure and enhance its resilience. Therefore, it was essential to determine the idle time at different damage levels. A statistical analysis was conducted on 33 discrete samples for each damage level to determine the relationship between idle time and the damage level. This analysis enabled a quantitative assessment of idle time at each specific damage level.

Table 6 lists the maximum, minimum, and mean idle times for tunnel sections at different damage levels, calculated using Eq. (1) based on expert responses. The idle time increased significantly as the damage level worsened. For example, when the tunnel was at a minor, moderate, extensive, or complete damage level, the mean values of the idle time were 6.52, 12.09, 24.02, and 50.57 d, respectively. From extensive to complete damage level, the mean value of idle time increased by 26.55 d, which is about 4.76 and 2.22 times the increment from minor to moderate damage level and from moderate to extensive damage level, respectively. In other words, the more severe the tunnel damage, the longer the preparatory work (e.g., inspection, condition assessment, and resource mobilization) required before rehabilitation can begin. Therefore, to expedite the repair of a damaged tunnel and prevent further deterioration, a timely emergency response is essential.

#### 3.2.2. Probabilistic models of idle time

Determining the quantitative probability of idle time for different damage levels enables a rescue department to devise a reliable restoration plan and effectively mobilize available resources. The methodology for constructing the probabilistic models of the maximum and minimum idle times was consistent with that used for the probabilistic models of the restoration time presented in Section 3.1.2. Fig. 6 shows the histograms for minimum and maximum idle times for different damage levels based on the collected discrete samples and their corresponding best-fit probability density function curves. It was found that, for the minimum idle time, the lognormal distribution best fits the minor damage level, the exponential distribution best fits the moderate damage level, and

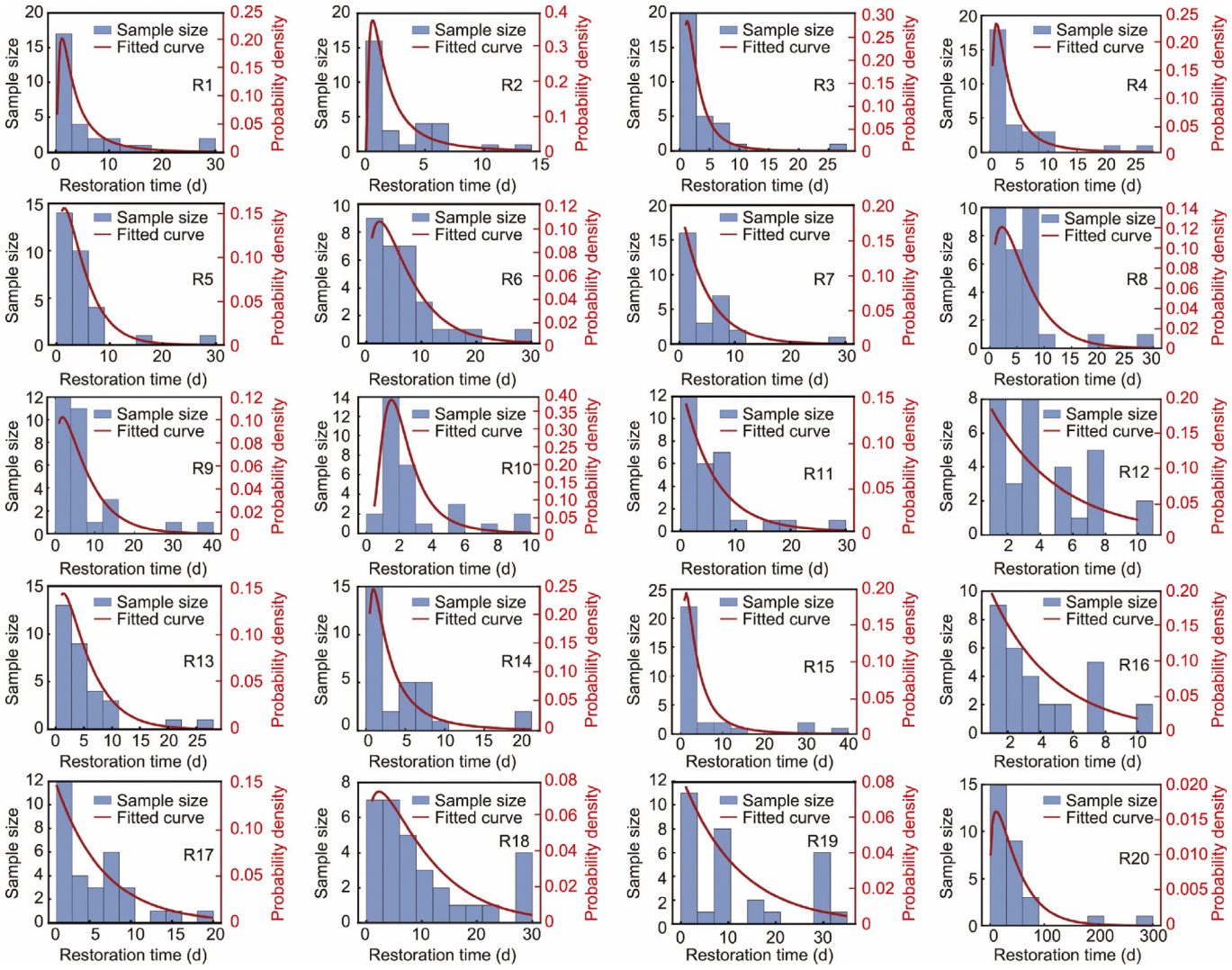


**Fig. 4.** Histograms and best-fit probability density function for the minimum restoration time of restoration tasks R1–R20.

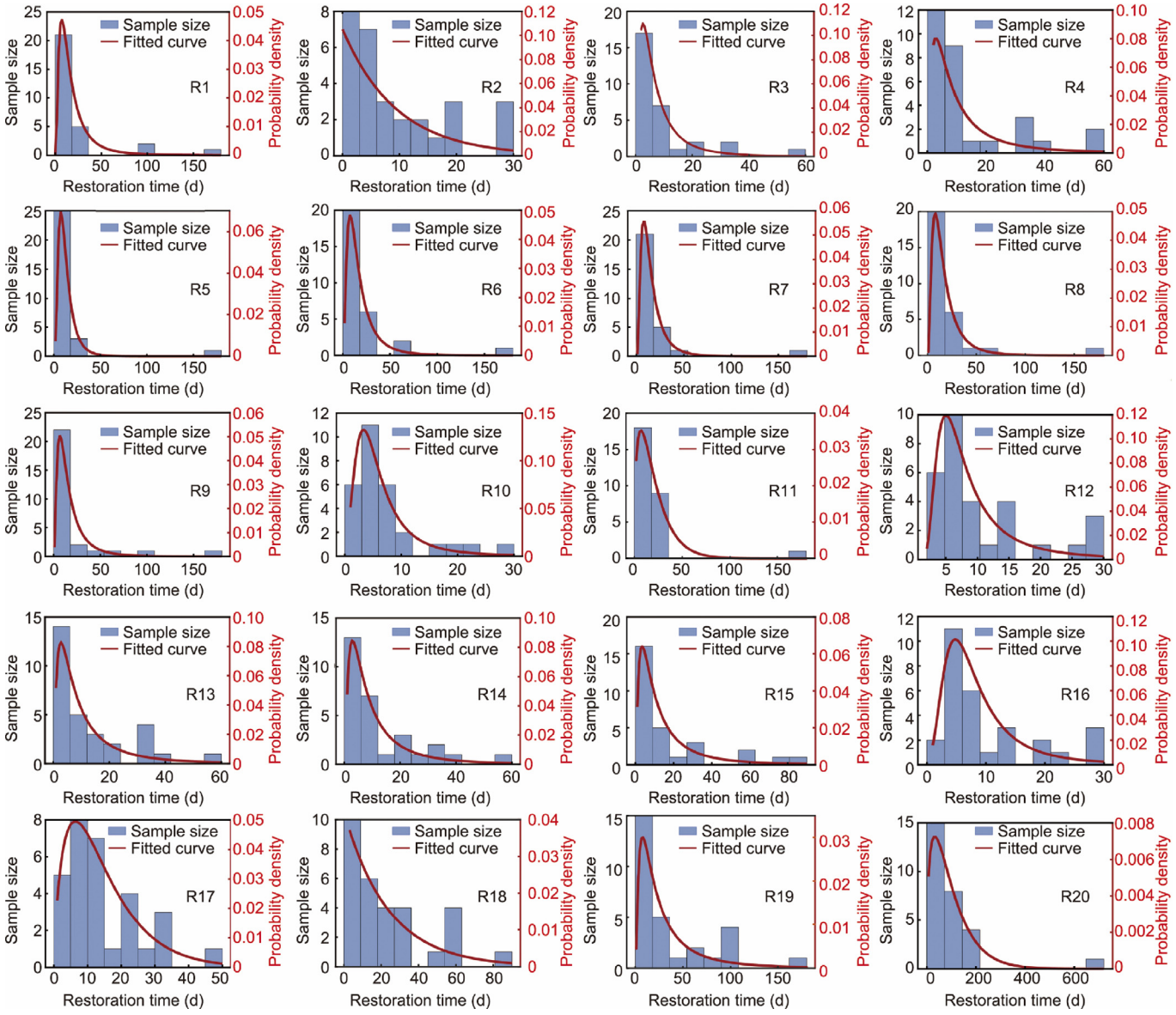


**Fig. 5.** Histograms and best-fit probability density function for the maximum restoration time of restoration tasks R1–R20.

**Table 4**
Key parameters of the fitted probability density functions for the minimum durations of restoration tasks.

| Restoration task | Distribution type | Numerical character | | Key parameter | | | | | |
|---|---|---|---|---|---|---|---|---|---|
| | | Mean | Standard deviation | $\mu$ | $\lambda$ | $\sigma$ | $k$ | $a$ | $b$ |
| R1 | Lognormal | 5.361 | 7.196 | 1.164 | — | 1.015 | — | — | — |
| R2 | Lognormal | 3.011 | 4.291 | 0.548 | — | 1.053 | — | — | — |
| R3 | Lognormal | 3.346 | 3.227 | 0.879 | — | 0.811 | — | — | — |
| R4 | Lognormal | 4.348 | 5.189 | 1.027 | — | 0.941 | — | — | — |
| R5 | Gamma | 4.701 | 3.905 | — | — | — | — | 1.449 | 3.244 |
| R6 | Gamma | 6.902 | 5.591 | — | — | — | — | 1.524 | 4.529 |
| R7 | Exponential | 4.810 | 4.810 | — | 4.810 | — | — | — | — |
| R8 | Gamma | 6.001 | 4.750 | — | — | — | — | 1.596 | 3.760 |
| R9 | Gamma | 7.244 | 6.263 | — | — | — | — | 1.338 | 5.414 |
| R10 | GEV | 2.511 | 1.801 | 1.707 | — | 0.959 | 0.211 | — | — |
| R11 | Exponential | 5.948 | 5.948 | — | 5.948 | — | — | — | — |
| R12 | Exponential | 4.239 | 4.239 | — | 4.239 | — | — | — | — |
| R13 | Gamma | 5.188 | 4.463 | — | — | — | — | 1.351 | 3.840 |
| R14 | Lognormal | 4.505 | 6.105 | 0.984 | — | 1.021 | — | — | — |
| R15 | Lognormal | 5.333 | 6.519 | 1.217 | — | 0.956 | — | — | — |
| R16 | Exponential | 3.933 | 3.933 | — | 3.933 | — | — | — | — |
| R17 | Exponential | 5.750 | 5.750 | — | 5.750 | — | — | — | — |

(*continued on next page*)

**Table 4** (*continued*)

| Restoration task | Distribution type | Numerical character | | Key parameter | | | | | |
|---|---|---|---|---|---|---|---|---|---|
| | | Mean | Standard deviation | $\mu$ | $\lambda$ | $\sigma$ | $k$ | $a$ | $b$ |
| R18 | Gamma | 10.013 | 8.802 | — | — | — | — | 1.294 | 7.738 |
| R19 | Exponential | 11.900 | 11.900 | — | 11.900 | — | — | — | — |
| R20 | Gamma | 46.025 | 40.044 | — | — | — | — | 1.321 | 34.841 |

$\mu$, $\lambda$, $\sigma$, $k$, $a$, and $b$ are parameters of probability density functions, with mathematical expressions provided in Table S6.

**Table 5**
Key parameters of the fitted probability density functions for the maximum durations of restoration tasks.

| Restoration task | Distribution type | Numerical character | | Key parameter | | | | | |
|---|---|---|---|---|---|---|---|---|---|
| | | Mean | Standard deviation | $\mu$ | $\lambda$ | $\sigma$ | $k$ | $a$ | $b$ |
| R1 | Lognormal | 20.377 | 20.940 | 2.654 | — | 0.849 | — | — | — |
| R2 | Exponential | 9.466 | 9.466 | — | 9.466 | — | — | — | — |
| R3 | Lognormal | 9.141 | 10.429 | 1.796 | — | 0.913 | — | — | — |
| R4 | Lognormal | 13.794 | 18.721 | 2.102 | — | 1.022 | — | — | — |
| R5 | Lognormal | 13.563 | 9.376 | 2.412 | — | 0.625 | — | — | — |
| R6 | Lognormal | 19.455 | 17.967 | 2.660 | — | 0.785 | — | — | — |
| R7 | Lognormal | 16.601 | 13.489 | 2.556 | — | 0.712 | — | — | — |
| R8 | Lognormal | 18.946 | 16.897 | 2.649 | — | 0.765 | — | — | — |
| R9 | Lognormal | 18.965 | 19.043 | 2.594 | — | 0.835 | — | — | — |
| R10 | GEV | 6.964 | 7.199 | 4.052 | — | 2.896 | 0.306 | — | — |
| R11 | Gamma | 20.570 | 16.784 | — | — | — | — | 1.502 | 13.695 |
| R12 | GEV | 10.765 | 19.839 | 6.155 | — | 3.359 | 0.451 | — | — |
| R13 | Lognormal | 13.607 | 18.820 | 2.076 | — | 1.034 | — | — | — |
| R14 | Lognormal | 12.744 | 16.521 | 2.052 | — | 0.993 | — | — | — |
| R15 | Lognormal | 17.562 | 24.482 | 2.326 | — | 1.039 | — | — | — |
| R16 | GEV | 9.529 | 9.208 | 5.770 | — | 3.783 | 0.300 | — | — |
| R17 | Gamma | 14.670 | 11.027 | — | — | — | — | 1.770 | 8.288 |
| R18 | Exponential | 23.700 | 23.700 | — | 23.700 | — | — | — | — |
| R19 | Lognormal | 37.246 | 51.433 | 3.084 | — | 1.033 | — | — | — |
| R20 | Gamma | 100.290 | 82.549 | — | — | — | — | 1.476 | 67.947 |

$\mu$, $\lambda$, $\sigma$, $k$, $a$, and $b$ are parameters of probability density functions, with mathematical expressions provided in Table S6.

**Table 6**
Minimum, maximum, and mean values of idle time per damage level for the examined tunnels.

| Damage level | Idle time (d) | | |
|---|---|---|---|
| | Minimum | Maximum | Mean |
| Minor | 2.90 | 10.14 | 6.52 |
| Moderate | 6.72 | 17.45 | 12.09 |
| Extensive | 13.66 | 34.38 | 24.02 |
| Complete | 28.24 | 72.90 | 50.57 |

the Gamma distribution best fits the extensive and complete damage levels. Additionally, the Gamma function is the best-fit function for the maximum idle time at most damage levels (minor, moderate, and extensive), while the lognormal function best fits it at the complete damage level. The numerical characteristics and key parameters of the best-fit probability density functions are listed in Tables 7 and 8, respectively.

### 3.3. Cost ratio

#### 3.3.1. Deterministic models of cost ratio

The cost ratio is a key economic indicator in the post-hazard restoration process of a damaged tunnel. Determining the cost ratio for a specific damage level can help owners and stakeholders to estimate restoration costs more effectively. Therefore, a deterministic assessment of cost ratios at various damage levels was conducted by statistically analyzing the discrete data provided by 33 experts, based on their engineering experience.

Table 9 lists the mean values of cost ratios for different damage levels. The pattern of variability in cost ratios was consistent with that of idle time. The more severe the tunnel damage, the higher the cost ratio. For example, the restoration of a tunnel with minor damage costs approximately 7.73% of the total construction cost, whereas restoring a tunnel with complete damage may cost as much as 74.05%.

#### 3.3.2. Probabilistic models of cost ratio

The actual restoration process involves numerous uncertainties, such as damage to restoration materials and unforeseen incidents, making it challenging to determine an exact cost ratio before completion. To address this, a probabilistic assessment of cost ratios was conducted using survey results. Probabilistic models of cost ratios were developed using the same methodology as in Sections 3.1.2 and 3.2.2. The corresponding histograms and best-fit probability density functions are shown in Fig. 7. It can be observed that the best-fit function for the cost ratio at extensive and complete damage levels follows a normal distribution. For moderate damage levels, the best-fit function is the GEV function with three parameters, and the best-fit function for minor damage follows a Gamma distribution. Table 10 summarizes the numerical characteristics and key parameters of the best-fit probability density functions in terms of legibility and ease of application.

### 3.4. Traffic reinstatement and capacity restoration

#### 3.4.1. Reinstatement models

To assess traffic capacity at different time points after the commencement of the rehabilitation task, expert evaluations of traffic-carrying capacity were collected at eight different time points for different damage levels. Among the 33 participating experts in

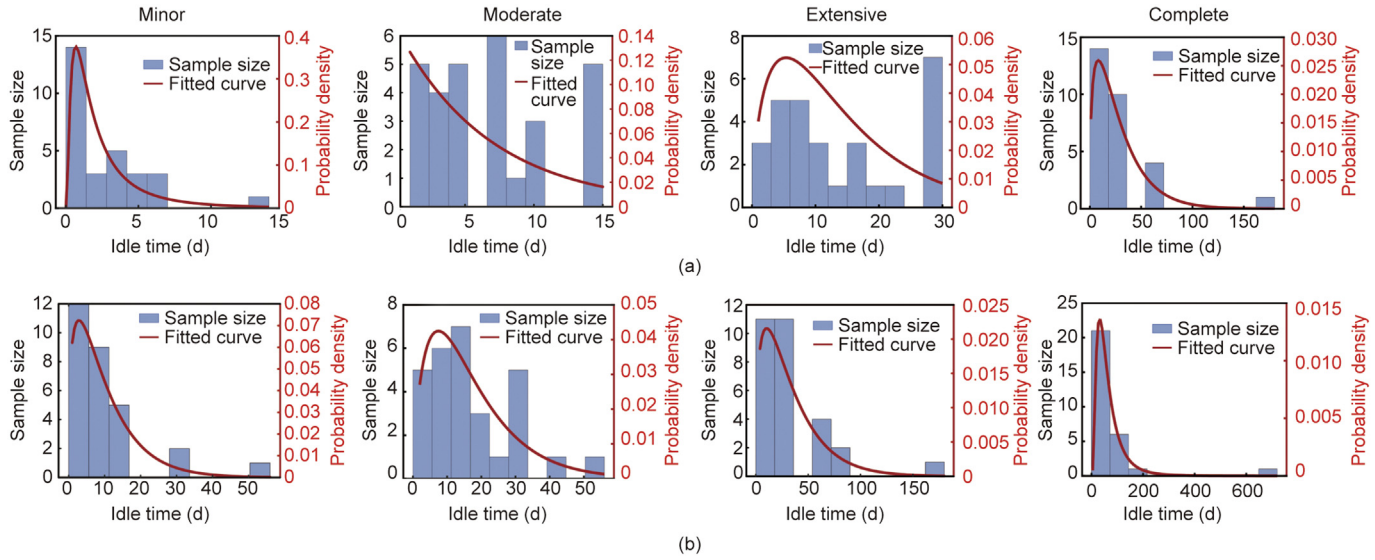


**Fig. 6.** Histograms and best-fit probability density function for the idle time at different damage levels. (a) Minimum idle time, (b) maximum idle time.

**Table 7**
Key parameters of the best-fit probability density functions for the minimum idle time at different damage levels.

| Damage level | Distribution type | Numerical character | | Key parameter | | | | | |
|---|---|---|---|---|---|---|---|---|---|
| | | Mean | Standard deviation | $\mu$ | $\lambda$ | $\sigma$ | $k$ | $a$ | $b$ |
| Minor | Lognormal | 2.822 | 3.538 | 0.565 | — | 0.972 | — | — | — |
| Moderate | Exponential | 6.817 | 6.817 | — | 6.817 | — | — | — | — |
| Extensive | Gamma | 13.813 | 10.793 | — | — | — | — | 1.638 | 8.433 |
| Complete | Gamma | 28.244 | 23.786 | — | — | — | — | 1.410 | 20.031 |

$\mu$, $\lambda$, $\sigma$, $k$, $a$, and $b$ are parameters of probability density functions, with mathematical expressions provided in Table S6.

**Table 8**
Key parameters of the best-fit probability density functions for the maximum idle time at different damage levels.

| Damage level | Distribution type | Numerical character | | Key parameter | | | | | |
|---|---|---|---|---|---|---|---|---|---|
| | | Mean | Standard deviation | $\mu$ | $\lambda$ | $\sigma$ | $k$ | $a$ | $b$ |
| Minor | Gamma | 10.138 | 8.602 | — | — | — | — | 1.389 | 7.299 |
| Moderate | Gamma | 16.805 | 12.725 | — | — | — | — | 1.774 | 9.636 |
| Extensive | Gamma | 33.834 | 28.195 | — | — | — | — | 1.440 | 23.496 |
| Complete | Lognormal | 68.182 | 55.499 | 3.968 | — | 0.713 | — | — | — |

$\mu$, $\lambda$, $\sigma$, $k$, $a$, and $b$ are parameters of probability density functions, with mathematical expressions provided in Table S6.

**Table 9**
Mean values of the cost ratio per damage level for the examined tunnels.

| Damage level | Cost ratio (%) |
|---|---|
| | Mean |
| Minor | 7.73 |
| Moderate | 20.39 |
| Extensive | 43.39 |
| Complete | 74.05 |

the questionnaire survey, 22 provided valid responses concerning traffic-carrying capacity. The statistical results of these expert assessments are shown in the histogram in Fig. 8. For example, in the case of a tunnel with minor damage, 10 d after the commencement of rehabilitation work, 19 experts assessed the traffic capacity to be fully restored at 100%, while three experts estimated it at only 50%. However, 60 d after the initiation of the rehabilitation work, all experts concurred that the traffic-carrying capacity had been fully restored to 100%. In addition, these histograms provide a visual representation of the variation in expert opinions regarding traffic capacity at different time points of the rehabilitation process.

Based on these statistics, the potential post-hazard gains in traffic capacity for various levels of tunnel damage were plotted, as shown in Fig. 9. The bold red lines represent traffic capacity values corresponding to the highest frequency in each histogram from Fig. 8, making them the most likely indicators of the real situation. In addition, the solid gray lines reflect the estimations provided by different experts, representing their individual judgments on the expected traffic capacity gain. It is evident that the more severe the damage level of the tunnel, the greater the number of distinct gain curves (i.e., the solid gray lines in Fig. 9) of the traffic capacity, resulting in increased uncertainty in restoring traffic capacity. For instance, there were five gain curves for minor damage, this number increased to 15 for tunnels that suffer complete damage.

Fig. 10 compares the gain in post-hazard traffic capacity obtained from the maximum frequency of histograms at different

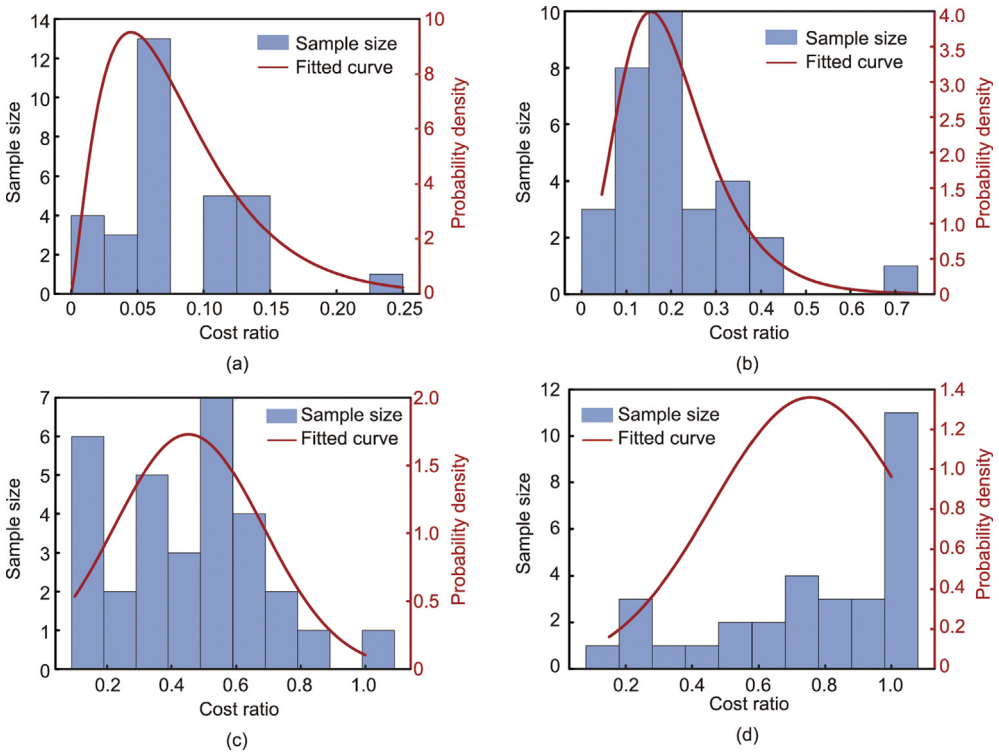


**Fig. 7.** Histograms and optimally fitted probability density function for the cost ratio at different damage levels: (a) minor, (b) moderate, (c) extensive, and (d) complete.

**Table 10**
Key parameters of the best-fit probability density functions for the cost ratios at different damage levels.

| Damage level | Distribution type | Numerical character | | Key parameter | | | | | |
|---|---|---|---|---|---|---|---|---|---|
| | | Mean | Standard deviation | $\mu$ | $\lambda$ | $\sigma$ | $k$ | $a$ | $b$ |
| Minor | Gamma | 0.079 | 0.052 | — | — | — | — | 2.310 | 0.034 |
| Moderate | GEV | 0.204 | 0.115 | 0.153 | — | 0.092 | –0.022 | — | — |
| Extensive | Normal | 0.453 | 0.231 | 0.453 | — | 0.231 | — | — | — |
| Complete | Normal | 0.756 | 0.293 | 0.756 | — | 0.293 | — | — | — |

$\mu$, $\lambda$, $\sigma$, $k$, $a$, and $b$ are parameters of probability density functions, with mathematical expressions provided in Table S6.

time points for different damage levels. It was observed that the more severe the damage level, the longer it takes to reinstate traffic capacity. For a tunnel with minor damage level, restoration to full operational capacity is achieved within 10 d. In contrast, for the completely damaged tunnel, it was not until 270 d after the commencement of the restoration work that the traffic-carrying capacity was restored to 100%. The established reinstatement (traffic capacity) model can be used to predict the recovery of traffic capacity by inputting the estimated damage levels from the fragility curves. This provides the authorities with a solid foundation for developing informed and effective post-disaster emergency plans.

*3.4.2. Capacity restoration models*

(1) **Deterministic models of capacity restoration.** Experts' judgments play a crucial role in selecting appropriate rehabilitation measures and in determining their prioritization. Fig. 11 shows the restoration task prioritization and expected duration of restoration tasks for different damage levels. Professional judgments on the sequence of importance of restoration tasks across all damage levels differ significantly. While some experts selected fewer tasks, R1 (regular monitoring and inspection of tunnel deformation data), R2 (detection of voids within or behind tunnel linings), R4 (tunnel leakage protection measures), and R12 (repair tunnel lining cracks) were commonly recognized as the most necessary tasks in most circumstances. By considering the shared tasks across the responses, the suggested model was able to balance various tasks and their expert-defined priorities using engineering judgment. To establish deterministic capacity restoration models, the estimated restoration time for each task was determined using the mean values listed in Table 3. Unsurprisingly, a longer restoration time is needed for the tunnel that suffers a greater degree of damage. The total restoration duration for tunnels with minor, moderate, extensive, and complete damage levels was 41.68, 59.44, 78.46, and 106.62 d, respectively. It was also observed that restoration tasks R1 and R2 were consistently applied across all damage levels, reinforcing the importance of regular monitoring and structural assessments in ensuring effective recovery.

The normalized post-earthquake structural capacity is defined as the ratio of the post-earthquake tunnel capacity ($Q_{pe}$) to the original capacity ($Q_0$). It is assumed that immediately after the hazard, the structural capacity ($Q$) is 0.9, 0.7, 0.4, and 0.1 for minor, moderate, extensive, and complete damage levels, respectively. That is, the corresponding loss of capacity is 10%, 30%, 60%, and 90%. Fig. 12(a) illustrates the matching deterministic stepwise restoration models corresponding to Fig. 11. To present a

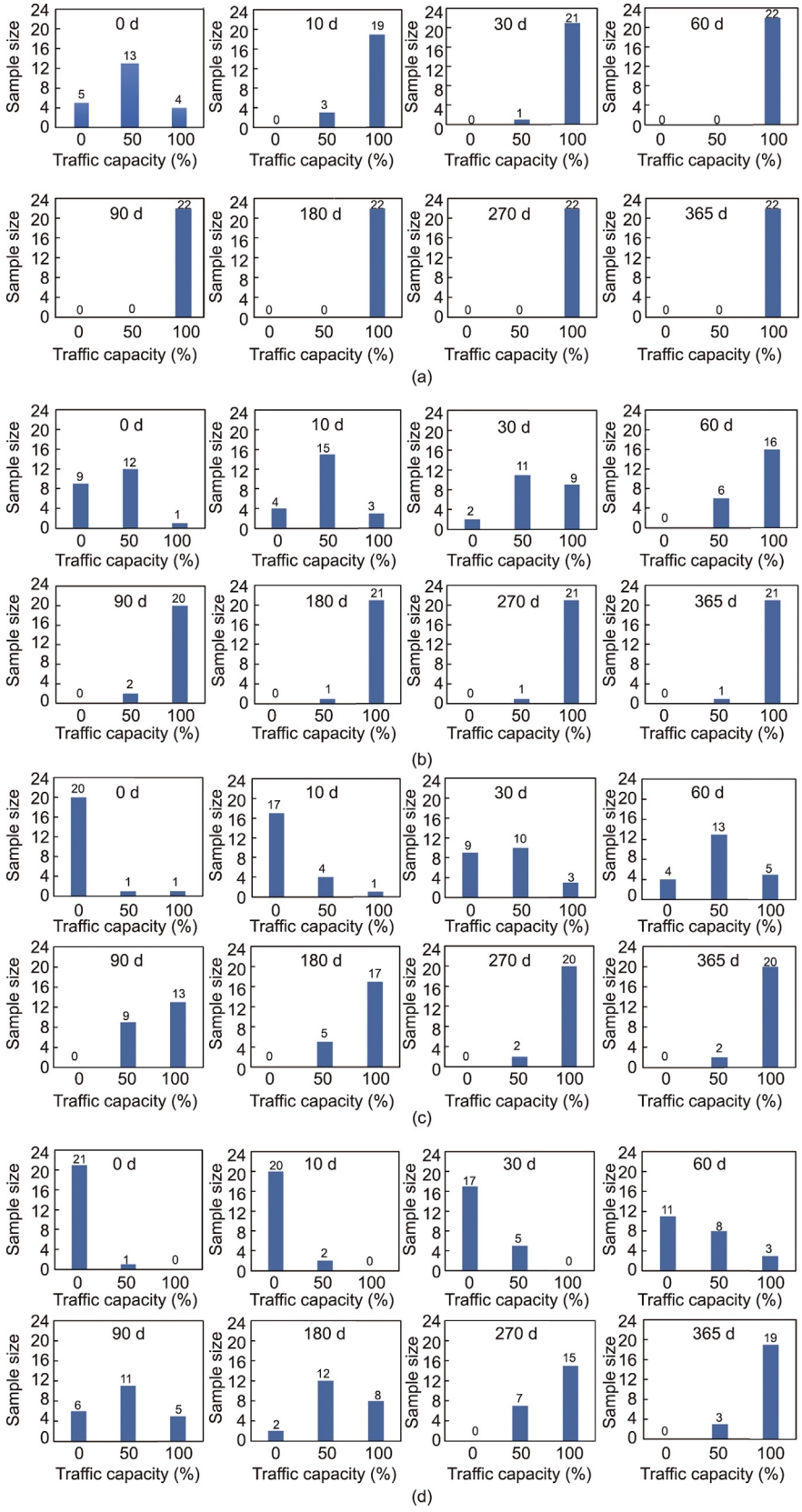


**Fig. 8.** Histograms of traffic-carrying capacity at eight time points after the hazard with different damage levels: (a) minor, (b) moderate, (c) extensive, and (d) complete.

continuous evolution of structural capacity, deterministic restoration models were developed by fitting the stepwise restoration models, as shown in Fig. 12(b). For ease of application, the fitting functions for the deterministic restoration models at different damage levels are listed in Table S7 in Appendix A. The stepwise restoration models correspond directly to different restoration

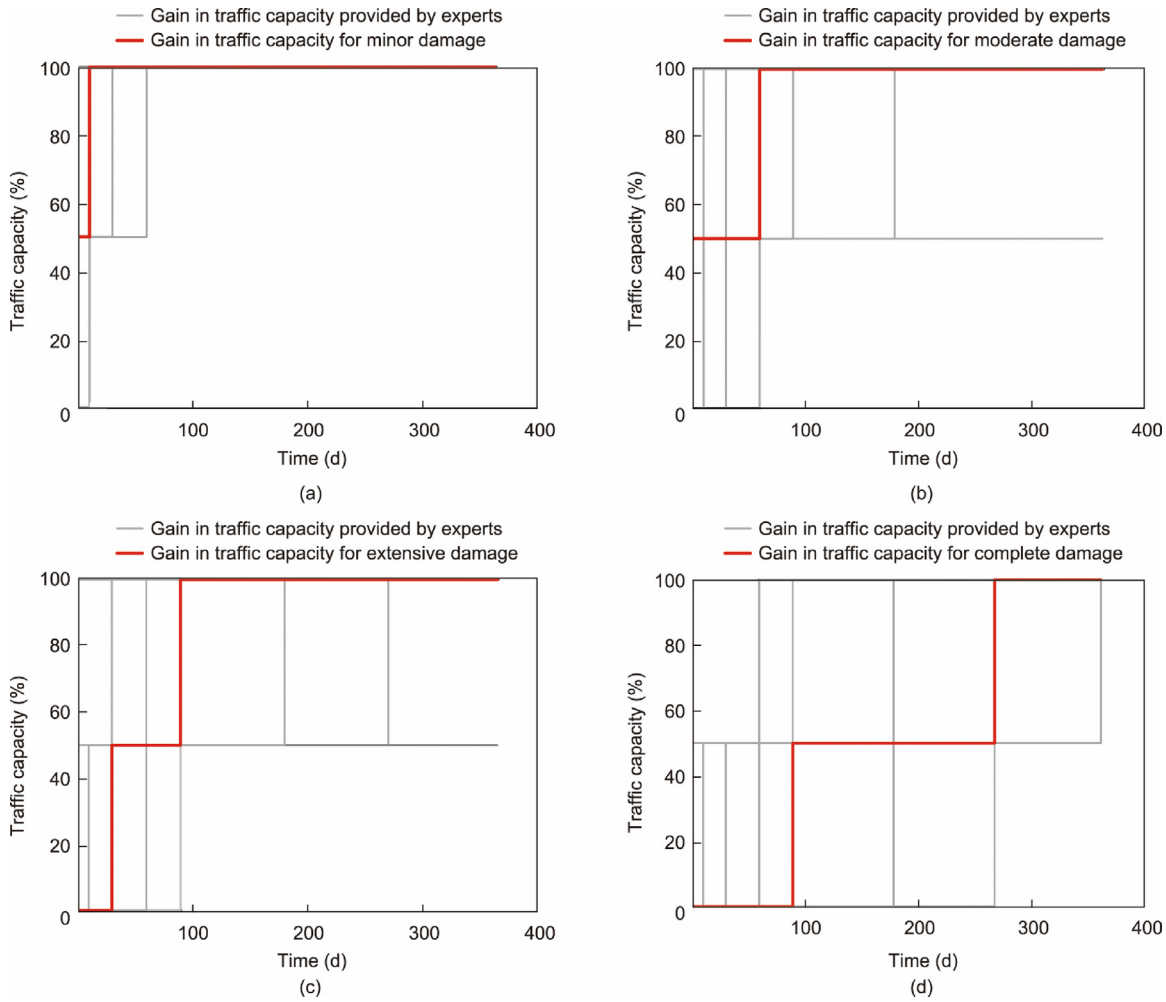


**Fig. 9.** Traffic capacity gain (%) for different damage levels of tunnels: (a) minor, (b) moderate, (c) extensive, and (d) complete.

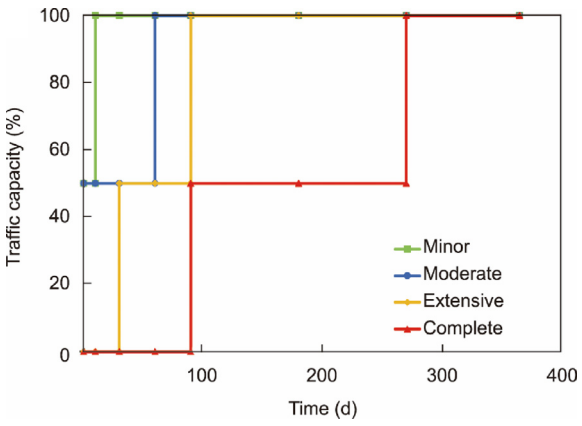


**Fig. 10.** Post-hazard traffic capacity gain (%) of tunnels.

tasks and their prioritization. The number of steps in the stepwise restoration model equals the number of restoration tasks performed, and the length of each step reflects the total duration of the corresponding task. Consistent with the rehabilitation information embodied in Fig. 11, greater damage levels require more rehabilitation tasks, leading to longer restoration durations. For minor, moderate, extensive, and complete damage levels, the post-hazard tunnel capacity can be restored to its original capacity within 45, 60, 80, and 110 d, respectively.

(2) **Probabilistic models of capacity restoration.** Due to the large amount of uncertainty in the restoration process, the duration of each task is not a fixed value. The restoration processes corresponding to Fig. 11 are used in this section to establish probabilistic capacity restoration models for different damage levels. Using the best-fit distribution, 10 000 samples were randomly selected for the duration of each restoration task. Note that the best-fit distributions for the maximum and minimum durations of each restoration tasks are not identical. Therefore, separate probabilistic stepwise capacity restoration models were developed based on the minimum and maximum durations of each restoration task, as shown in Figs. 13 and 14. Since tunnel rehabilitation is a continuous process, probability stepwise models were fitted to reflect the continuous evolution of post-disaster tunnel capacity, as shown in Figs.15 and 16. These continuous functions allow for the prediction of post-disaster structural capacity at any time point. The fitting functions for the mean values of the probabilistic restoration curves (red solid lines in Figs.14 and 16) can be obtained from Tables S8 and S9 in Appendix A. It is apparent from Fig. 13 that the time required to restore capacity at minor, moderate, extensive, and complete damage levels is highly likely to be less than 50, 60, 80, and 100 d, respectively. In other words, the more severe the damage level, the higher the probability that it will take more time to restore capacity. Additionally, the more severe the damage level, the wider the distribution range of possible stepwise capacity restoration curves, indicating greater uncertainty in the restoration process. Similarly, the probabilistic

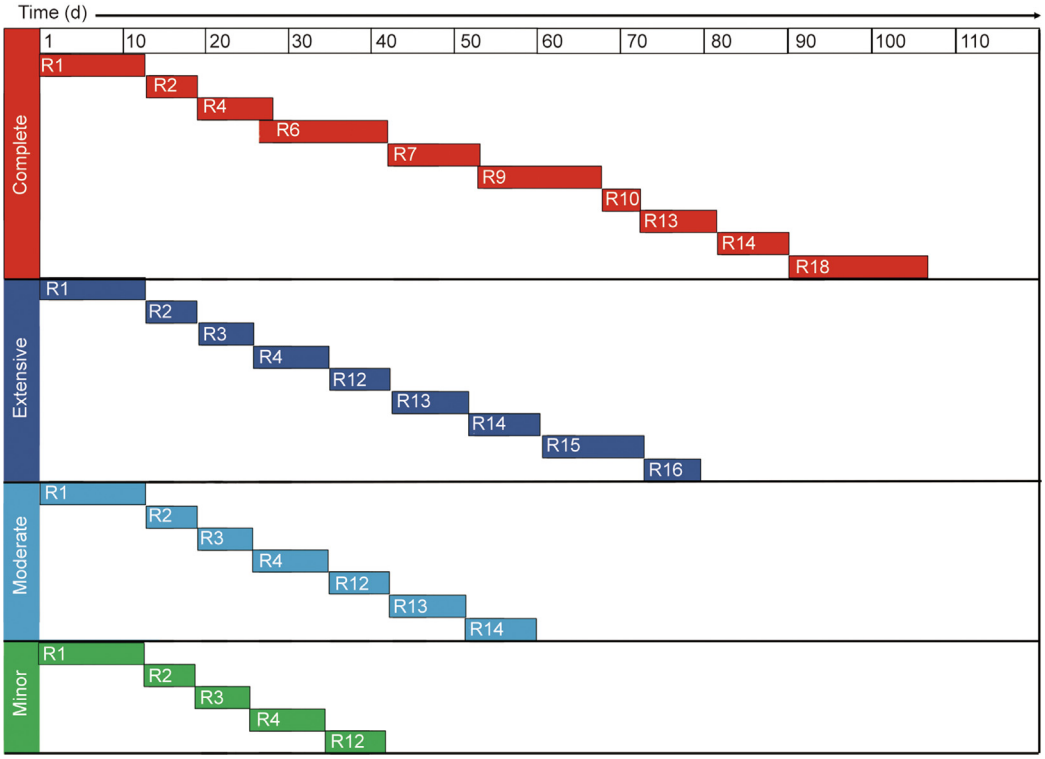


**Fig. 11.** Restoration task prioritization and durations per damage level.

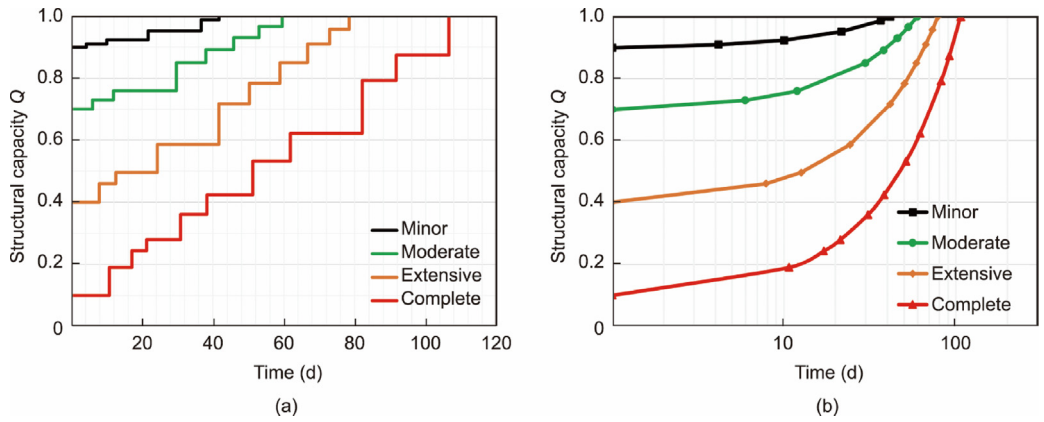


**Fig. 12.** Deterministic restoration models illustrating the post-hazard tunnel capacity. (a) Stepwise restoration models; (b) continuous restoration models.

stepwise capacity restoration models based on the maximum duration of each restoration task reflect the same pattern, as shown in Fig. 14.

## 4. Application of the developed tunnel restoration models

### *4.1. Description of the examined tunnels and corresponding vulnerability curves*

To highlight the application of the developed restoration models for tunnel resilience assessment, typical subway tunnels constructed using the shield tunneling method were examined in cases of seismic damage. The examined tunnel was constructed using an earth pressure balance (EPB) shield machine with a typical circular-shaped cross-section composed of segmental lining. The outer diameter of the lining ring was 6 m, and its wall thickness was 0.3 m. The burial depth (i.e., the distance from the ground surface to the tunnel crown) was 9 m, and the tunnel was in strata composed of silty clay and clay. Further details about the examined tunnel are available in the study by Zou et al. [106]. In this study, a detailed seismic vulnerability assessment of the tunnels was conducted, focusing on the seismic performance of the segments and joints. The seismic fragility curves of the examined tunnels using PGA as IM, were also obtained, as shown in Fig. 17 [106].

Based on these fragility curves, the probability of the examined tunnel being subjected to a certain damage level for different seismic intensities can be calculated using Eqs. (2) and (3).

$$P(\mathrm{DS}_i|\mathrm{IM}) = P(\mathrm{DS} > \mathrm{DS}_{i+1}|\mathrm{IM}) - P(\mathrm{DS} > \mathrm{DS}_i|\mathrm{IM}),\ \text{for}\ i = 1-3 \quad (2)$$

$$P(\mathrm{DS}_i|\mathrm{IM}) = P(\mathrm{DS} > \mathrm{DS}_i|\mathrm{IM}),\ \text{for}\ i = 4 \quad (3)$$

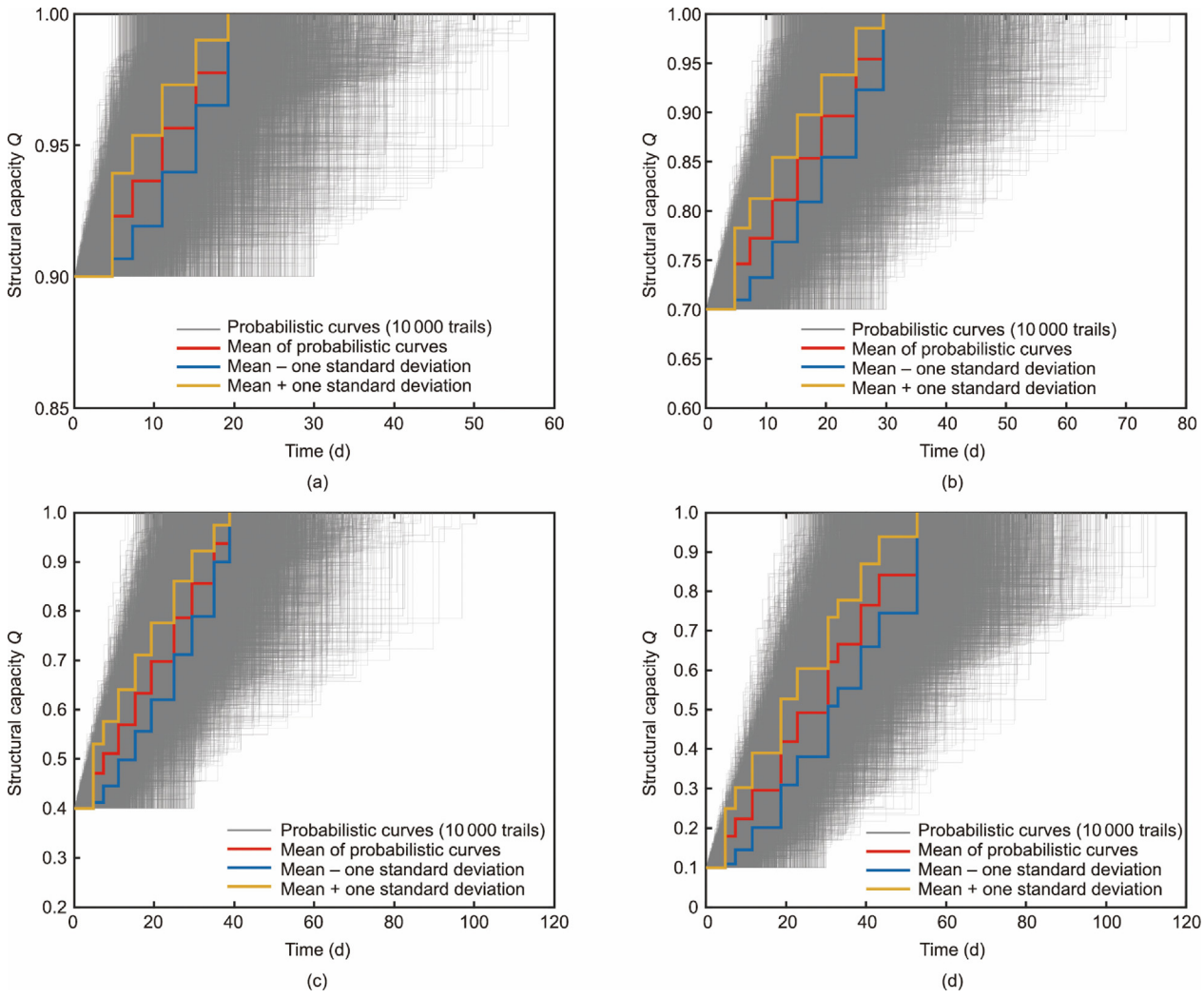


**Fig. 13.** Probabilistic stepwise capacity restoration models based on the minimum restoration time under (a) minor, (b) moderate, (c) extensive, and (d) complete damage levels.

where $P(\mathrm{DS}_i|\mathrm{IM})$ represents the probability of the tunnel being in a specific DS ($\mathrm{DS}_i$) at a given seismic intensity. $P(\mathrm{DS} > \mathrm{DS}_i|\mathrm{IM})$ is the probability of the damage exceeding a $\mathrm{DS}_i$, which can be obtained directly from the fragility curves. $\mathrm{DS}_1$, $\mathrm{DS}_2$, $\mathrm{DS}_3$, and $\mathrm{DS}_4$ corresponds to minor, moderate, extensive, and complete damage levels, respectively.

### 4.2. Cost of the analyzed tunnels

Based on the fragility curves by Zou et al. [106] and the cost models developed in this study, the normalized costs ($C$) of the examined tunnels under different earthquake intensities can be calculated using Eq. (4) [107].

$$C = \sum_{i=1}^{4} P(\mathrm{DS}_i|\mathrm{IM})C_i \tag{4}$$

where $P(\mathrm{DS}_i|\mathrm{IM})$ can be calculated using Eqs. (2) and (3). $C_i$ represents the cost ratio for different DSs, as described in Section 3.3.

Based on the best-fit distribution of cost ratios for different damage levels given in Section 3.3.2, 10 000 discrete samples of cost ratios were randomly selected for each damage level. The corresponding 10 000 weighted cost ratios were subsequently calculated by considering all possible damage levels for a given hazard intensity, using the corresponding damage probabilities defined by the fragility curves. Fig.18 illustrates the probabilistic and deterministic loss assessments under different values of PGA. As the seismic intensity increases, the normalized cost also increases. Specifically, when PGA is less than 0.2$g$, the normalized cost is almost close to zero; however, at a PGA of 1.6$g$, the normalized cost may reach 0.9. In addition, higher seismic intensities are associated with greater uncertainty in the normalized cost. This phenomenon can be attributed to the fact that more severe damage levels correspond to greater uncertainty in the cost ratio.

### 4.3. Resilience assessment of the examined tunnels

#### 4.3.1. Resilience assessment method

The resilience assessment method adopted in this study aligns with the works of Argyroudis et al. [40], Pang and Wang [108], and Zhou et al. [109], as introduced briefly below. First, to develop resilience curves at different seismic intensities, the tunnel capacity at different time points was determined using Eq. (5) [107,110].

$$Q(t|\mathrm{IM}) = \sum_{i=0}^{4} Q(\mathrm{DS}_i|t)P(\mathrm{DS}_i|\mathrm{IM}) \tag{5}$$

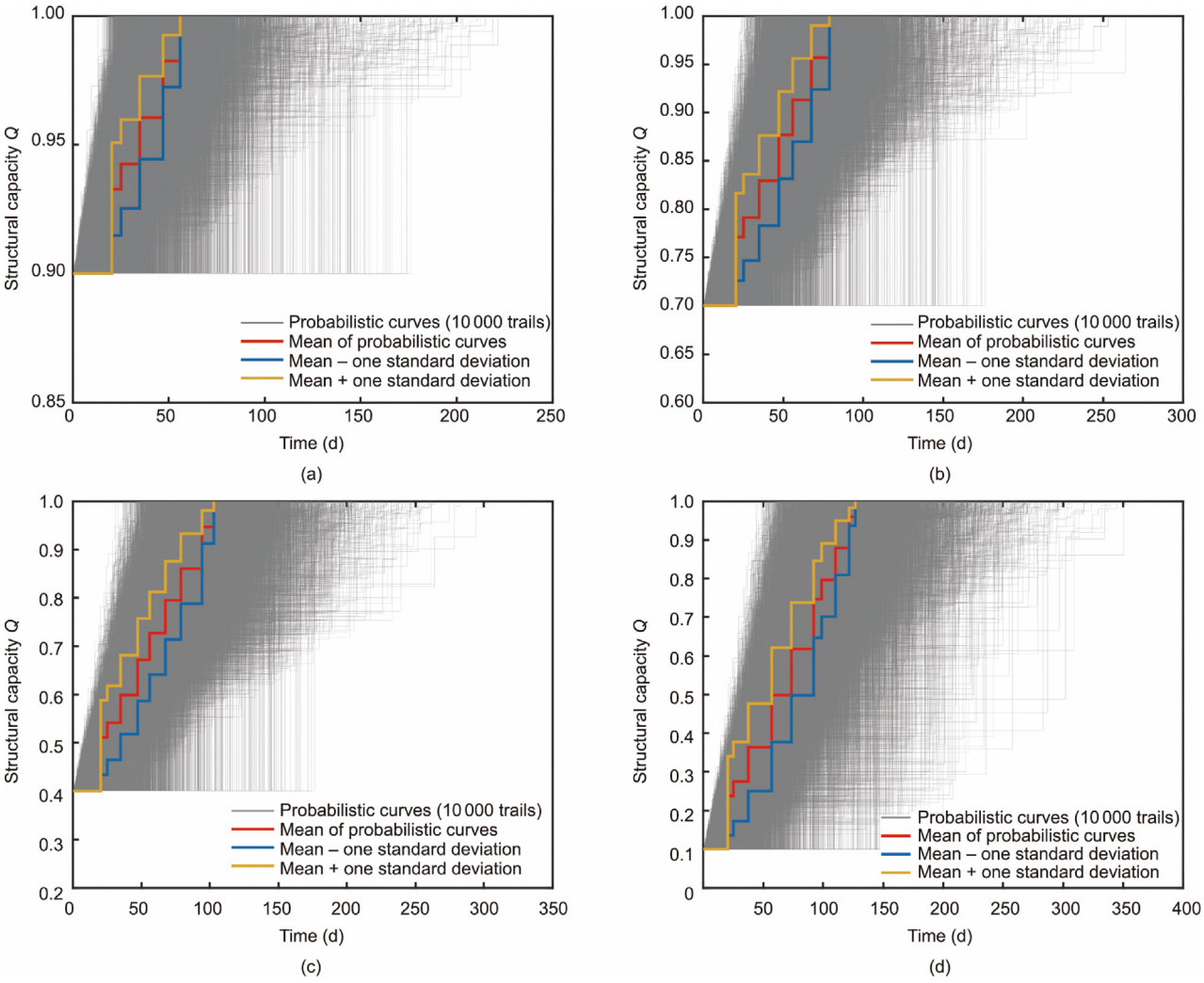


**Fig. 14.** Probabilistic stepwise capacity restoration models based on the maximum restoration time under (a) minor, (b) moderate, (c) extensive, and (d) complete damage levels.

where $Q(\mathrm{DS}_i|t)$ is the structural capacity of the tunnel at time $t$ in the $\mathrm{DS}_i$, as shown in Section 3.4, and $P(\mathrm{DS}_i|\mathrm{IM})$ follows the formulation in Eq. (4).

Apart from the restoration time, idle time, weighted by the probability of occurrence for each DS, is also considered a variable affecting rapidity in the resilience curves. The idle times for different seismic intensities ($I(\mathrm{IM})$) can be calculated using Eq. (6).

$$I(\mathrm{IM}) = \sum_{i=0}^{4} I(\mathrm{DS}_i) P(\mathrm{DS}_i|\mathrm{IM}) \tag{6}$$

where $I(\mathrm{DS}_i)$ represents the idle time of the tunnel in the $\mathrm{DS}_i$, which can be obtained from Table 6 or random sampling based on the best-fit distribution. $P(\mathrm{DS}_i|\mathrm{IM})$ is consistent with that in the previous formula.

After developing the resilience curves for different seismic intensities, the corresponding resilience indices were calculated using Eq. (7) [71,107,111,112].

$$Re = \frac{1}{t_h - t_0} \int_{t_0}^{t_h} Q(t)\mathrm{d}t \tag{7}$$

where $Re$ is the resilience index, $t_0$ is the time of the earthquake occurrence ($t_0$ is set as 0 in this study), $t_h$ is the control time ($t_h$ is set as 365 d in this study), $t$ is the time variable, and $Q(t)$ is the structural capacity of the examined tunnel at time $t$, as shown in Eq. (5).

#### 4.3.2. Resilience assessment based on the deterministic capacity restoration model

Fig. 19(a) illustrates the recovery of the structural capacity of the examined tunnel under different PGA values. It was observed that the larger the value of PGA, the more time it takes for the functionality of the tunnel to fully recover. This phenomenon occurs because as the damage level increases, both the idle time and duration of each restoration task also increase. This observation aligns with previously drawn conclusions.

Fig. 19(b) presents the evolution of the resilience index for the examined tunnel under different PGA values. When the PGA is less than 0.2$g$, the resilience index is close to 1.0, meaning that the tunnel is in a good functional state. However, the seismic resilience index gradually decreases for PGA values greater than 0.2$g$. This decline in resilience becomes more pronounced when PGA exceeds 0.8$g$ and slows upon reaching 1.2$g$. Specifically, when PGA was increased from 0$g$ to 1.6$g$, the resilience index decreased from 1.0 to 0.75. Overall, the resilience index decreases as seismic intensity (i.e., PGA) increases.

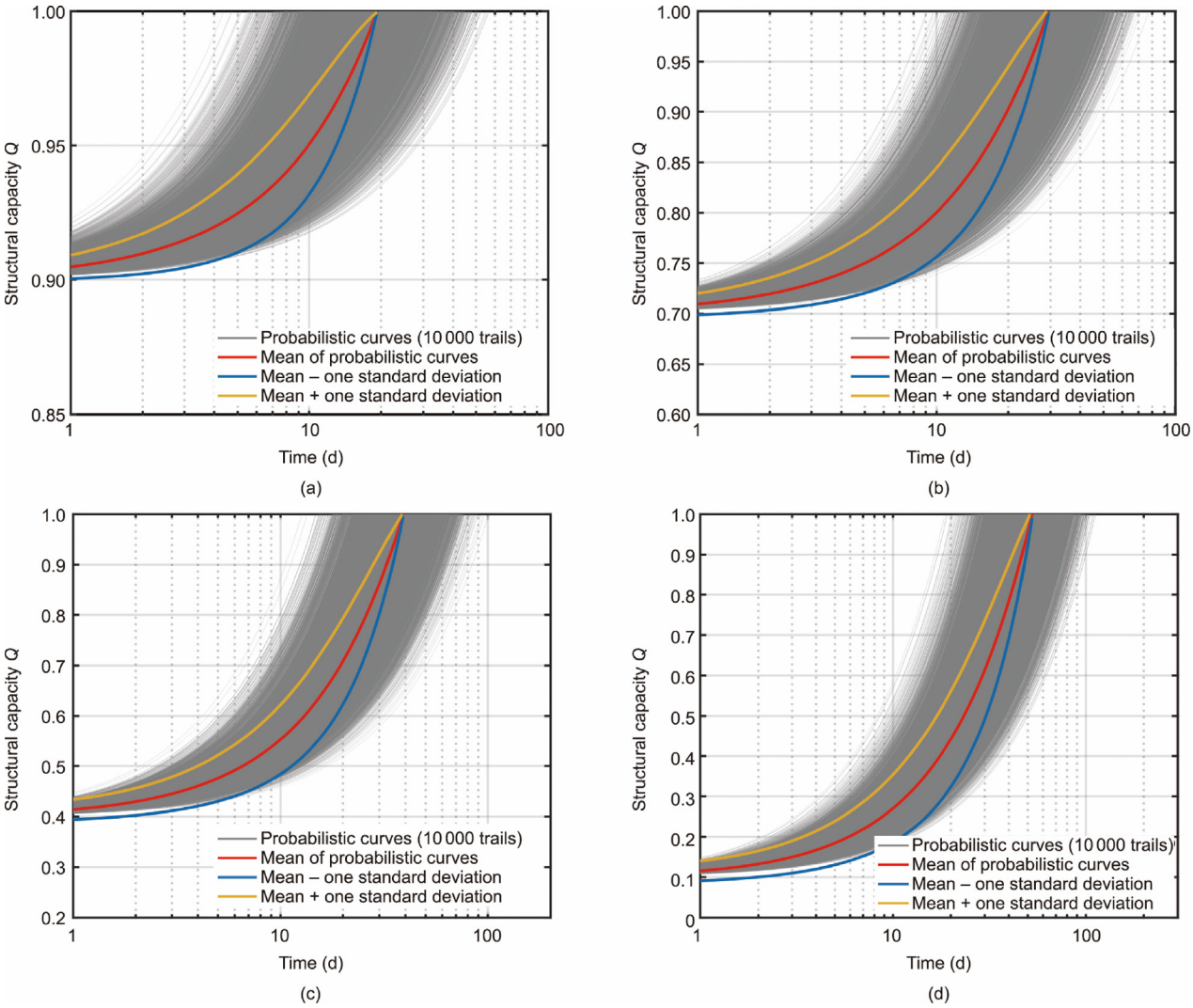


**Fig. 15.** Probabilistic continuous capacity restoration models based on the minimum restoration time under (a) minor, (b) moderate, (c) extensive, and (d) complete damage levels.

*4.3.3. Resilience assessment based on the probabilistic capacity restoration model*

It has been emphasized that there is a great deal of uncertainty in the restoration process, which leads to variability in the idle time, capacity of the tunnel at the same time point, and the time required to complete the entire restoration process. To account for this uncertainty, probabilistic resilience curve profiles were created by weighing the capacities of the examined tunnels at different damage levels based on probabilistic capacity restoration models. Similarly, after plotting 10 000 probabilistic resilience curves under a given PGA value, corresponding 10 000 resilience indices were obtained using Eq. (7).

To analyze the impact of restoration time (including idle time) on tunnel resilience, the probabilistic stepwise capacity restoration models shown in Figs. 13 and 14 were used to quantify the upper and lower bounds of the resilience index. Figs. 20(a)–(c) show the probabilistic resilience curves for PGA values of 0.2*g*, 0.5*g*, and 1.0*g* when both the duration of restoration tasks and idle time are at their minimum values. When the PGA is 0.2*g*, the restoration time for the tunnel capacity is within 0 to 50 d. At a PGA of 0.5*g*, this period extends from 0 to 90 d, and at 1.0*g*, it further extends to 130 d. Not surprisingly, the time required to fully repair the structural capacity of the examined tunnel increases significantly when both the duration of each restoration task and idle time reach their maximum values, as shown in Figs. 21(a)–(c).

Figs. 22(a) and (b) show the probabilistic resilience index *Re* of the examined tunnel in terms of PGA, based on minimum and maximum restoration times. As illustrated in Fig. 22, the resilience index decreases with increasing seismic intensity (i.e., PGA), with the rate of decline initially accelerating and then slowing. The pattern of evolution is consistent with the conclusions from the deterministic resilience assessment described in Section 4.3.2. In contrast to the deterministic analysis, the probabilistic resilience assessment fully captures the uncertainty of the resilience index at different PGA values. As PGA increases, the uncertainty in the resilience index also rises, as evidenced by the broader distribution ranges. For instance, under minimum restoration time conditions, the probabilistic resilience index ranges from 0.9787 to 0.9973 at a PGA of 0.5*g*, and extends from 0.8996 to 0.9763 at a PGA of 1.0*g*, with the latter interval being approximately 4.12 times broader. In addition, the probabilistic resilience index based on maximum restoration time shows more significant uncertainty than that based on minimum restoration time. Specifically, at a PGA of 1.6*g*, the probabilistic resilience index based on maximum restoration time ranges from 0.3643 to 0.9097, whereas that based on the minimum restoration time ranges from 0.5734 to 0.9656.

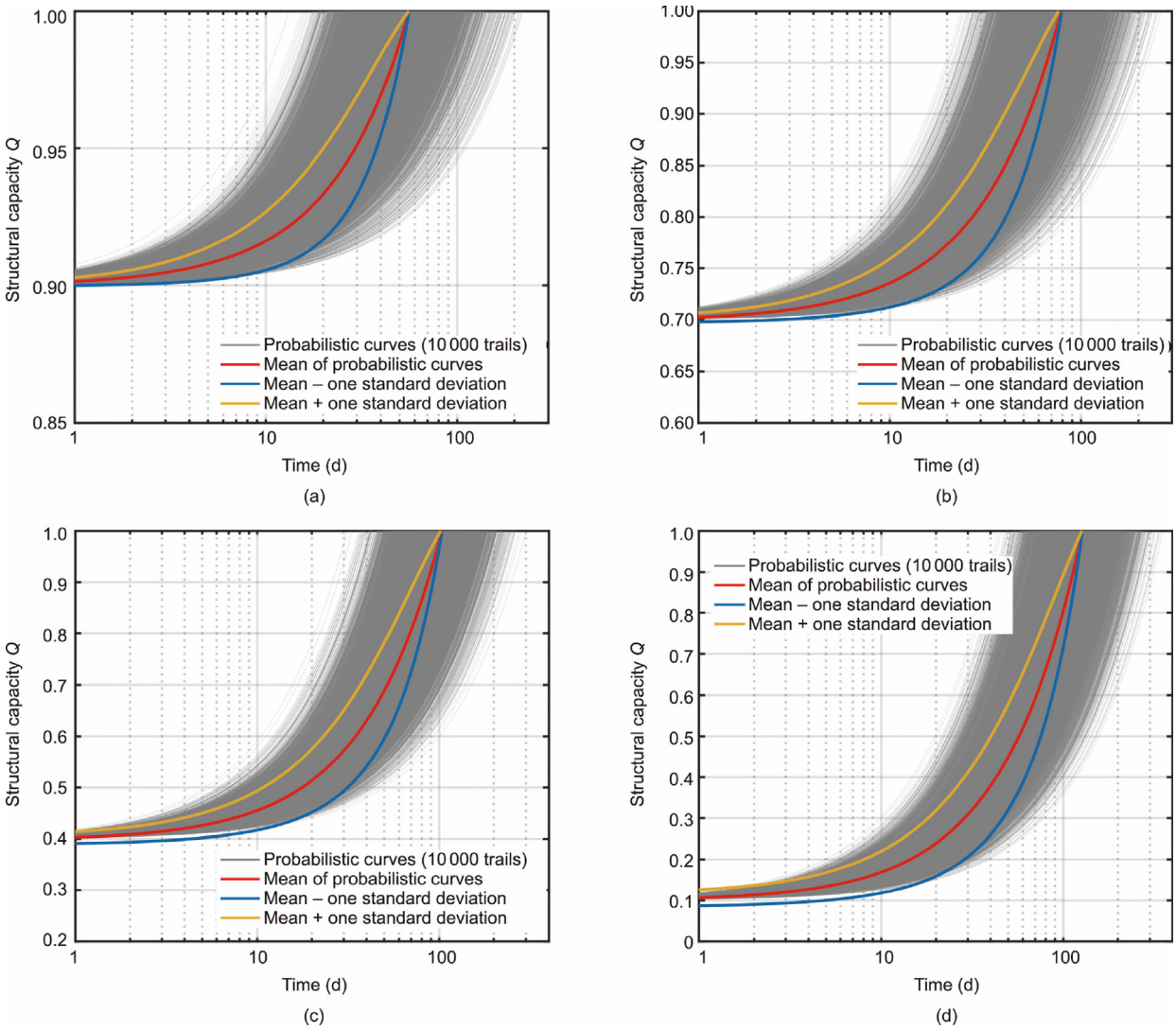


**Fig. 16.** Probabilistic continuous capacity restoration models based on the maximum restoration time under (a) minor, (b) moderate, (c) extensive, and (d) complete damage levels.

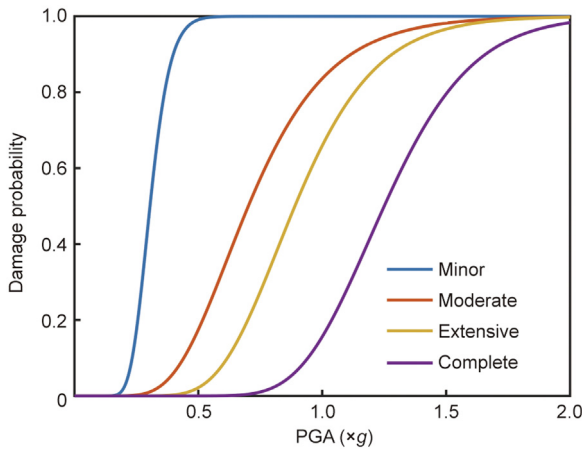


**Fig. 17.** Fragility functions of the examined tunnels by Zou et al. [106].

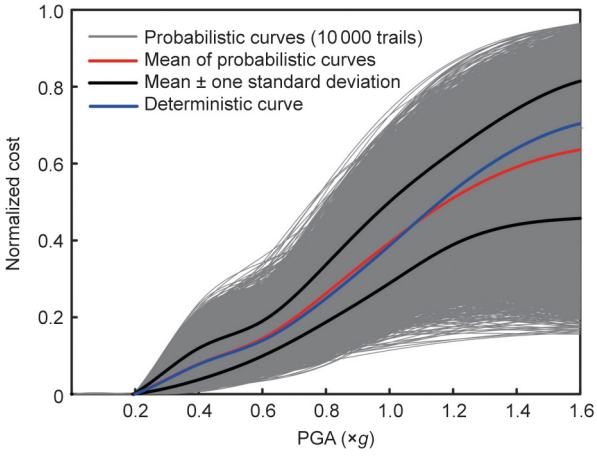


**Fig. 18.** Evolution of the normalized cost with the seismic intensity.

The increased uncertainty is attributed to the higher variability in the maximum duration for each repair task, as reflected in the standard deviation presented in Table 5. In general, the results of both deterministic and probabilistic resilience assessments support resilience-informed decisions for pre-event planning and post-event response strategies.

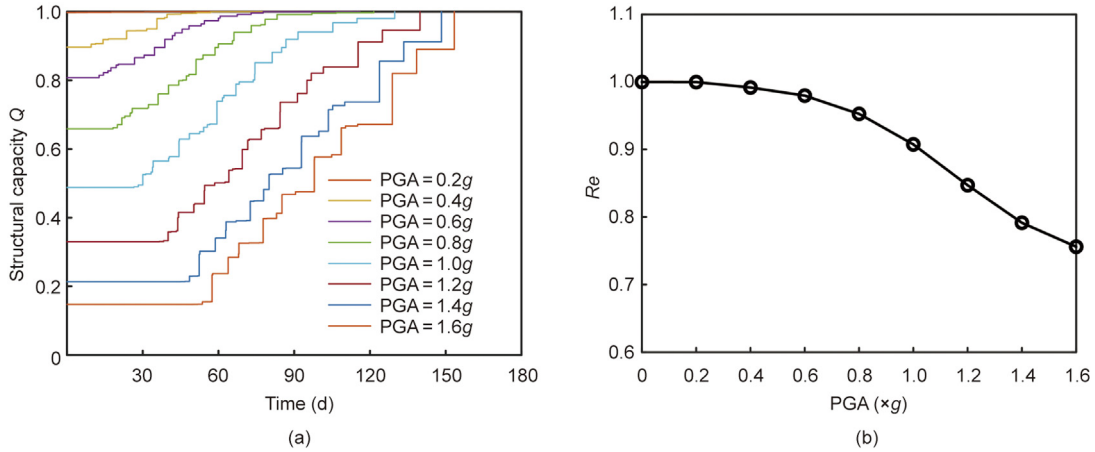


**Fig. 19.** Structural capacity recovery and resilience assessment for examined tunnels. (a) Resilience curves for different seismic intensities. (b) Resilience index *Re* of the examined tunnel in terms of PGA.

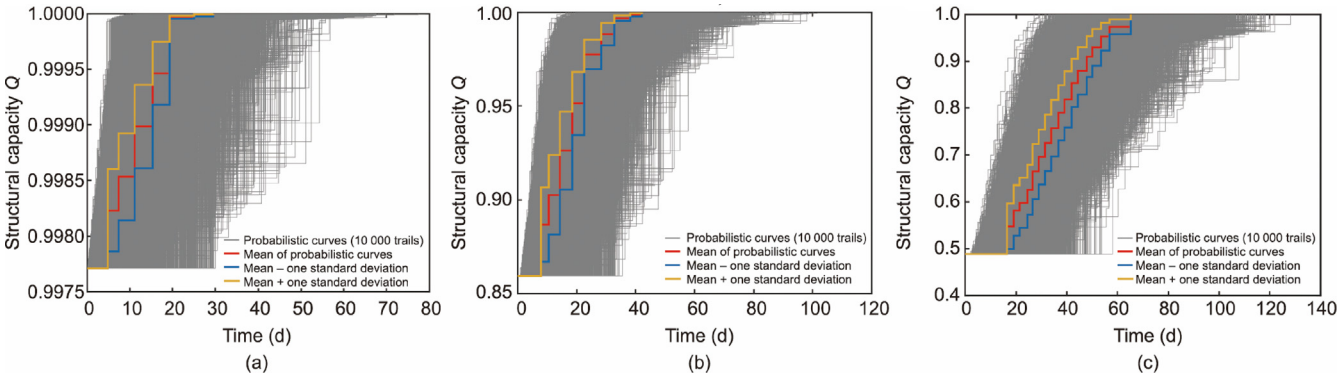


**Fig. 20.** Probabilistic resilience curves for PGA values of (a) 0.2*g*, (b) 0.5*g*, and (c) 1.0*g* based on the minimum restoration time.

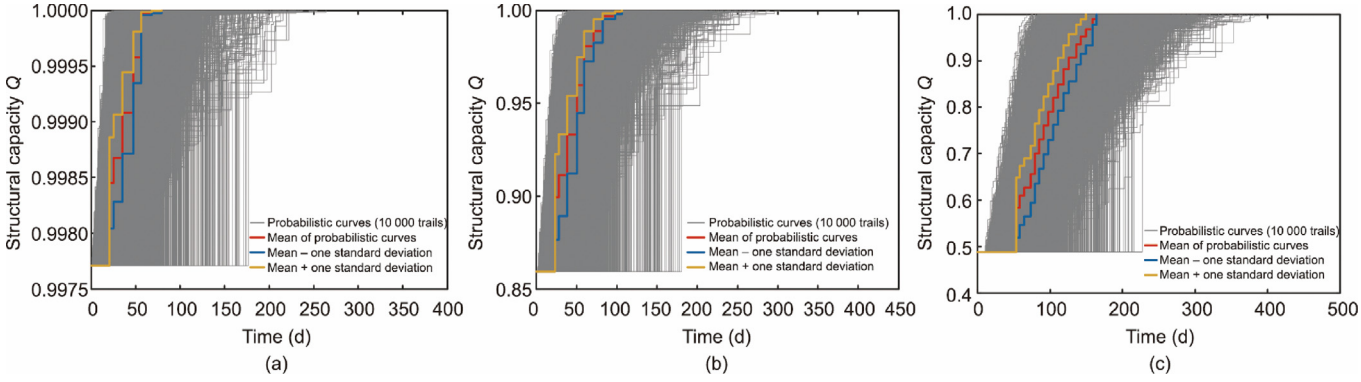


**Fig. 21.** Probabilistic resilience curves for PGA values of (a) 0.2*g*, (b) 0.5*g*, and (c) 1.0*g* based on the maximum restoration time.

#### *4.3.4. Sensitivity analysis of expert opinions on resilience index outputs*

Given the inherent subjectivity embedded in expert judgment, potential cognitive biases may directly affect the output of the established resilience models. As an illustrative case, a sensitivity analysis was conducted on the probabilistic resilience model based on maximum restoration time. Expert-derived estimates of maximum uncertainty time parameters tend to exhibit greater variability, as previously discussed. Specifically, the resilience indices were compared by varying input parameters through the following modifications: ① changing the mean values (±30%, ±20%, and ±10%) of the probability distributions for both idle time and restoration task durations; ② adjusting the standard deviations (±30%, ±20%, and ±10%) of the respective distributions, and ③ implementing simultaneous perturbations to both mean values and standard deviations (±30%, ±20%, and ±10%). The mean value adjustments account for systematic overestimation or underestimation of idle time and restoration durations by experts, while variations in standard deviation reflect the extent of dispersion int expert opinions.

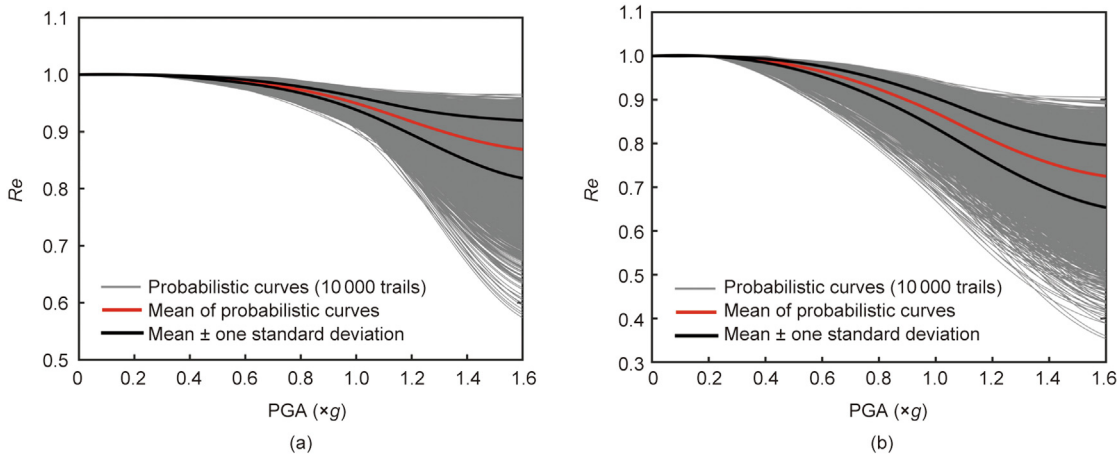


**Fig. 22.** Probabilistic resilience index of the examined tunnel in terms of PGA based on the (a) minimum restoration time and (b) maximum restoration time.

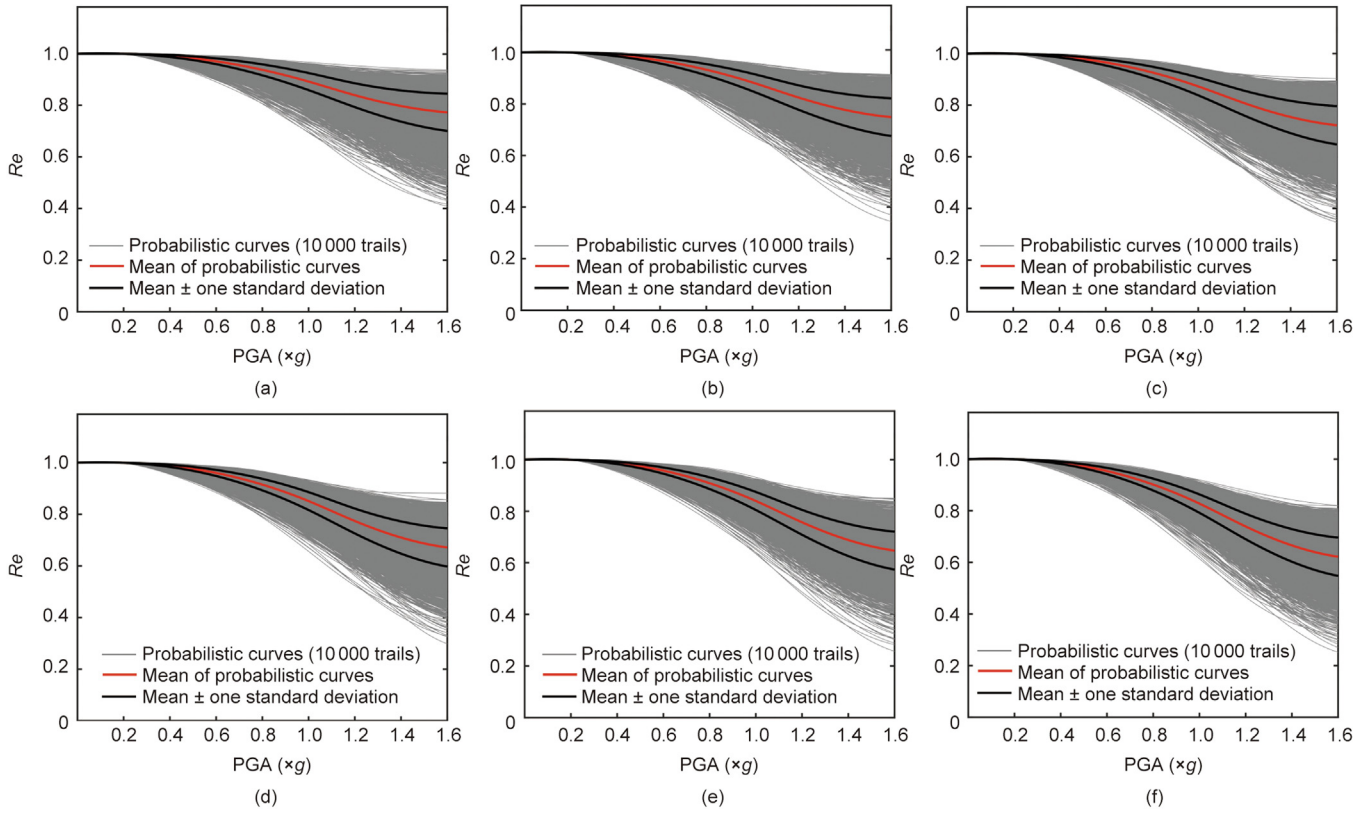


**Fig. 23.** Probabilistic resilience indices response to mean adjustments by (a) –30%, (b) –20%, (c) –10%, (d) 10%, (e) 20%, and (f) 30%.

Figs. 23–25 show the sensitivity of probabilistic resilience index responses to changes in mean values, standard deviation, and their concurrent variations. To better visualize variations in resilience model outcomes, Table 11 presents a comparison of the maximum, minimum, mean, and standard deviation values of resilience indices at PGA values of 0.5*g*, 1.0*g*, and 1.6*g*. When experts overestimate temporal variability during the post-earthquake restoration, the mean values of their fitted probability distributions increase. This upward shift in the mean values leads to an overall reduction in resilience index outputs. This trend is visually reflected in the continuous downward shift of the red solid line in Fig. 23. Quantitative analysis indicates that at a PGA of 1.6*g*, a 30% reduction in distribution means results in a resilience index of 0.7728, whereas a 30% increase lowers it to 0.6218. As shown in Fig. 24, an increase in the standard deviation of expert opinion probability distributions corresponds to a wider dispersion in the probabilistic resilience index. This trend becomes particularly pronounced at higher PGA levels. For instance, at a PGA of 1.6*g*, decreasing the standard deviation by 30% constrains the probabilistic resilience index to a range of 0.4106–0.8585, whereas increasing it by 30% expands the range to 0.2582–0.9194. Hence, greater consistency among expert estimations of idle time and restoration duration results in more precise resilience index predictions for tunnels under specific seismic intensities. Consistent with engineering judgment, when both the mean and standard deviation of the probability distributions for the resilience model

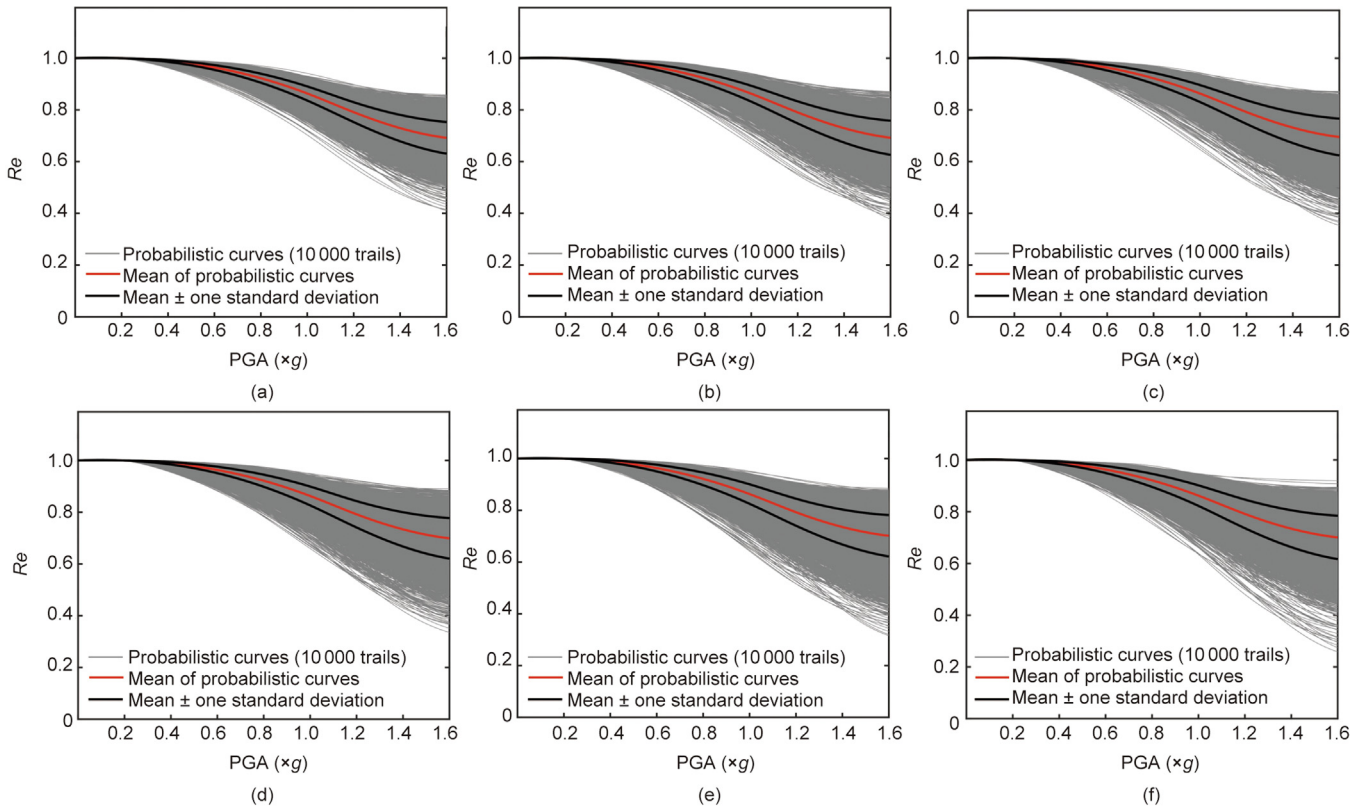


**Fig. 24.** Probabilistic resilience indices response to standard deviation adjustments by (a) −30%, (b) −20%, (c) −10%, (d) 10%, (e) 20%, and (f) 30%.

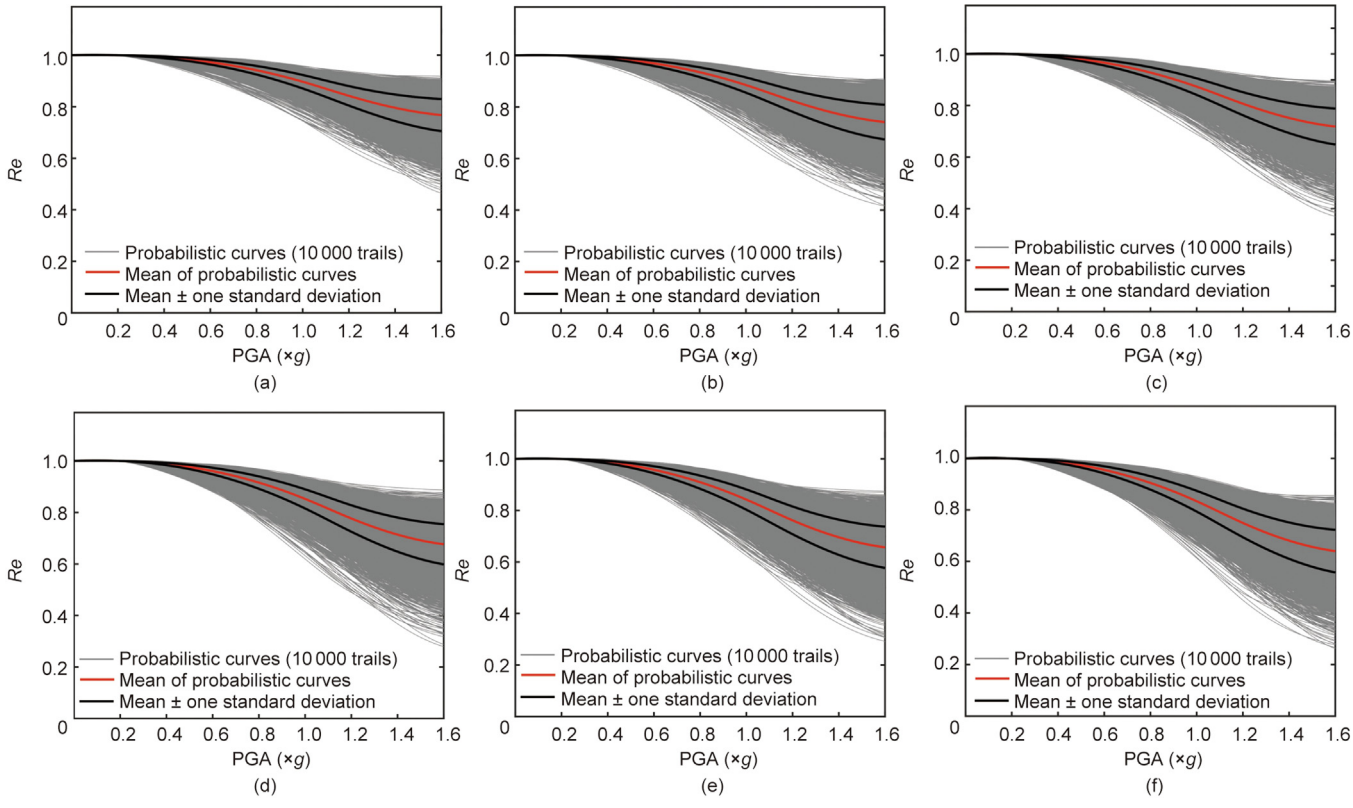


**Fig. 25.** Probabilistic resilience indices response to simultaneous mean and standard deviation adjustments by (a) −30%, (b) −20%, (c) −10%, (d) 10%, (e) 20%, and (f) 30%.

**Table 11**
Variation in resilience index outputs.

| Parameter in probability distributions | Change (%) | Resilience index output | | | | | | | | | | | |
|---|---|---|---|---|---|---|---|---|---|---|---|---|---|
| | | PGA = 0.5*g* | | | | PGA = 1.0*g* | | | | PGA = 1.6*g* | | | |
| | | Maximum | Minimum | Mean | Standard deviation | Maximum | Minimum | Mean | Standard deviation | Maximum | Minimum | Mean | Standard deviation |
| Mean | −30 | 0.9954 | 0.9267 | 0.9825 | 0.0071 | 0.9672 | 0.6940 | 0.8921 | 0.0331 | 0.9373 | 0.4084 | 0.7728 | 0.0721 |
| | −20 | 0.9956 | 0.9272 | 0.9810 | 0.0074 | 0.9590 | 0.6773 | 0.8832 | 0.0339 | 0.9150 | 0.3443 | 0.7488 | 0.0732 |
| | −10 | 0.9943 | 0.9238 | 0.9795 | 0.0076 | 0.9453 | 0.6646 | 0.8731 | 0.0346 | 0.9032 | 0.3461 | 0.7223 | 0.0742 |
| | 10 | 0.9926 | 0.9219 | 0.9761 | 0.0076 | 0.9336 | 0.6563 | 0.8513 | 0.0346 | 0.8817 | 0.2979 | 0.6715 | 0.0740 |
| | 20 | 0.9918 | 0.9147 | 0.9743 | 0.0077 | 0.9313 | 0.6347 | 0.8396 | 0.0345 | 0.8499 | 0.2567 | 0.6472 | 0.0735 |
| | 30 | 0.9907 | 0.9135 | 0.9724 | 0.0078 | 0.9198 | 0.6143 | 0.8279 | 0.0357 | 0.8206 | 0.2515 | 0.6218 | 0.0742 |
| Standard deviation | −30 | 0.9916 | 0.9326 | 0.9783 | 0.0060 | 0.9410 | 0.7031 | 0.8635 | 0.0272 | 0.8585 | 0.4106 | 0.6920 | 0.0611 |
| | −20 | 0.9924 | 0.9292 | 0.9781 | 0.0066 | 0.9366 | 0.6816 | 0.8632 | 0.0230 | 0.8884 | 0.3816 | 0.6928 | 0.0654 |
| | −10 | 0.9923 | 0.9230 | 0.9780 | 0.0073 | 0.9435 | 0.6469 | 0.8632 | 0.0327 | 0.8718 | 0.3535 | 0.6953 | 0.0711 |
| | 10 | 0.9938 | 0.9209 | 0.9778 | 0.0081 | 0.9491 | 0.6595 | 0.8625 | 0.0364 | 0.8906 | 0.3353 | 0.6988 | 0.0784 |
| | 20 | 0.9942 | 0.9211 | 0.9778 | 0.0084 | 0.9510 | 0.6421 | 0.8626 | 0.0377 | 0.8850 | 0.3154 | 0.7014 | 0.0799 |
| | 30 | 0.9942 | 0.9141 | 0.9777 | 0.0086 | 0.9469 | 0.6346 | 0.8620 | 0.0396 | 0.9194 | 0.2582 | 0.7005 | 0.0839 |
| Mean and standard deviation | −30 | 0.9950 | 0.9350 | 0.9835 | 0.0059 | 0.9583 | 0.7443 | 0.8968 | 0.0262 | 0.9189 | 0.4642 | 0.7674 | 0.0623 |
| | −20 | 0.9938 | 0.9260 | 0.9815 | 0.0066 | 0.9517 | 0.6780 | 0.8849 | 0.0296 | 0.9088 | 0.4156 | 0.7414 | 0.0674 |
| | −10 | 0.9942 | 0.9270 | 0.9796 | 0.0071 | 0.9474 | 0.6885 | 0.8733 | 0.0320 | 0.8951 | 0.3693 | 0.7185 | 0.0700 |
| | 10 | 0.9920 | 0.9205 | 0.9762 | 0.0082 | 0.9390 | 0.6193 | 0.8526 | 0.0372 | 0.8871 | 0.2793 | 0.6765 | 0.0781 |
| | 20 | 0.9922 | 0.9136 | 0.9745 | 0.0088 | 0.9310 | 0.6245 | 0.8418 | 0.0393 | 0.8744 | 0.2916 | 0.6567 | 0.0802 |
| | 30 | 0.9918 | 0.9175 | 0.9732 | 0.0089 | 0.9303 | 0.6130 | 0.8338 | 0.0402 | 0.8561 | 0.2615 | 0.6401 | 0.0827 |

input parameters increase simultaneously, the resilience index exhibits a decline in magnitude along with heightened uncertainty.

## 5. Discussion

The development of resilience models relies on a probabilistic framework incorporating expert survey insights. This approach is based on the following assumptions: ① The damaged tunnel is of average importance, meaning that no additional human or financial resources are allocated for its restoration. The potential impact of transportation restrictions on resource delivery is not considered. ② The ageing of the tunnel does not affect its structural capacity. Therefore, before the hazard event, the structural capacity of the tunnel is assumed to be 1.0. However, immediately after the hazard, the post-hazard capacity decreases to 0.9, 0.7, 0.4, and 0.1 for the minor, moderate, extensive, and complete damage levels, respectively, based on expert judgment. ③ The DS of non-structural components (i.e., electromechanical equipment and rail tracks) is consistent with that of the main structure (i.e., the tunnel lining) and is not determined through fragility curves. ④ The restoration process of the damaged tunnel is considered to be continuous, without interruptions due to factors such as weather or management issues. ⑤ After the implementation of all repair measures, the structural capacity of the tunnel is fully restored to its original level, that is, $Q = 1.0$.

The established tunnel resilience models can be effectively incorporated into resilience-based post-earthquake restoration workflows, guiding practitioners in optimal decision-making. This decision-making process incorporates recovery and reinstatement time estimates, based on which downtime and losses due to disruption can be estimated more accurately using the models presented in this paper. This framework facilitates proactive tunnel adaptation [113], aiming to reduce losses and accelerate recovery through optimized post-hazard measures. The steps for integrating this model into resilience planning workflows are as follows: ① The developed resilience models can be employed by tunnel operators or policymakers to predict the resilience index of tunnels under various seismic intensities. Based on the resilience index, the resilience state of tunnel structures can then be determined. ② Restoration workflows, derived from expert surveys and post-earthquake restoration practices under similar conditions, can be referenced. These workflows help determine a technically feasible and economically viable restoration strategy while considering costs. ③ Expert opinion-based resilience assessment methods can be leveraged by decision-makers to evaluate resilience indices of tunnel structures under various post-earthquake restoration scenarios involving different restoration tasks and implementation sequences. This approach enables the identification of the most sensitive temporal parameters affecting resilience states, thereby facilitating the sensitivity-informed optimization of restoration strategies. For instance, allocating additional resources to shorten the duration of dominant repair tasks can effectively enhance the speed of post-earthquake recovery. In summary, the proposed framework facilitates investment prioritization and optimal resource allocation by systematically comparing the resilience of structures and cost–benefit trade-offs across various restoration strategies. This methodology provides quantifiable metrics to enhance preparedness, response, and recovery planning while supporting compliance with evolving infrastructure resilience standards and policies [114,115].

Future research should focus on enhancing the reliability and generalizability of the restoration models by collecting more expert responses, covering a wider range of countries and regions. Additionally, weighting methods such as the analytic hierarchy process (AHP) and the entropy method can be used to account for the differences between estimates derived from actual data from previous case studies and those based on professional judgment, assigning varying levels of importance to each estimate based on its source and reliability [116,117]. To mitigate cognitive biases and improve the robustness of resilience models, a Bayesian probabilistic framework can be adopted to update the probability distributions of expert opinions dynamically by incorporating objective data derived from engineering practice [118]. Moreover, a structured Delphi method with iterative anonymous feedback can be implemented to enhance consensus formation while minimizing individual dominance [119]. Because resilience models are directly influenced by tunnel design objectives, configurations, and geological conditions, restoration models can be further developed to be flexible and adaptable. This can be achieved by incorporating parameters that can be tailored to specific tunnel designs, such as lining thickness, burial depth, and material properties. Adjustment factors can also be introduced to account for variables, such as operator policies, available resources, tunnel importance, and global effects, including the financial growth of different coun-

tries. Nonstructural factors also significantly influence the restoration process. Extreme weather events, such as rainfall and temperature fluctuations, affect tunnel integrity and subsequent restoration procedures. The geographical location of tunnels, including factors such as proximity to water bodies or areas prone to natural disasters, influences restoration strategies and timelines. Therefore, future studies should employ geospatial analysis and environmental modeling to assess the impact of these nonstructural factors. To facilitate this, more detailed data on weather conditions and tunnel locations should be obtained through collaboration with meteorological agencies and the application of geographic information systems (GISs). Furthermore, tunnel functionality degradation due to factors such as rebar corrosion can be accounted for, allowing for the development of restoration models for tunnels with varying service lives and construction quality. More importantly, the residual structural capacities of tunnels at different damage levels must be quantified through numerical simulations or experimental studies to establish more accurate restoration models.

## 6. Conclusions

This study delivered the first quantitative resilience model based on an extensive expert questionnaire for a benchmark circular tunnel under natural hazards. The developed restoration models reflect the recovery pathways of post-hazard tunnel capacity under different damage levels, bridging the gap in restoration modeling by quantifying the resilience of tunnels and considering the uncertainty of the restoration process. The following conclusions were drawn from this study:

(1) Due to the variations in expert professional backgrounds and differences in design cultures and standards across countries and regions, inherent biases exist in experts' responses to the questionnaire. These regional and cognitive biases are reflected in the standard deviations of key restoration process variables, such as restoration time, idle time, and cost ratios. As the severity of the tunnel damage increases, the standard deviation of these key variables increases, making it more challenging to identify appropriate probability distributions that fit these variables effectively. The deterministic models are used for practical applications, while the probabilistic models characterize epistemic uncertainties. The established restoration models accurately reflect the recovery of the post-disaster structural capacity from the perspective of the tunnel structure itself, and based on this, a resilience assessment of the tunnel structure was conducted. The rapid recovery of tunnel functionality can significantly contribute to the restoration of transportation network connectivity, thereby enhancing overall transportation network resilience. In addition, tunnel restoration models provide valuable guidance for resource allocation in disaster-affected areas. By systematically analyzing rehabilitation needs, these models help decision-makers formulate rational resource distribution strategies and optimize resource allocations, thus improving the efficiency and effectiveness of recovery efforts.

(2) The most time-consuming restoration tasks involve the replacement of structural components or reinforcement of tunnel linings and adjacent soil strata. Expert estimations suggest that idle time and cost ratios increase significantly with greater damage severity, with higher uncertainty in cost ratios at more extreme damage levels. Regarding the traffic capacity following the damage, this study indicates that more severe damage leads to lower post-event traffic capacity and longer restoration times. Typical restoration pathways are established for different damage levels to guide the process of restoring the traffic-carrying capacity. Appropriate rehabilitation measures can be taken, and their prioritization can be adjusted to achieve rapid restoration of traffic-carrying capacity. Continuous restoration models, obtained by fitting stepwise restoration models, reflect the continuity of post-hazard tunnel capacity restoration. Finally, a case study of a typical tunnel was conducted to illustrate the application of these restoration models for seismic resilience assessment.

## CRediT authorship contribution statement

**Zhong-Kai Huang:** Writing – review & editing, Writing – original draft, Validation, Software, Resources, Methodology, Investigation, Formal analysis, Data curation, Conceptualization. **Nian-Chen Zeng:** Writing – original draft, Methodology. **Dong-Mei Zhang:** Writing – review & editing, Visualization, Validation, Supervision, Resources, Project administration, Methodology, Investigation, Funding acquisition. **Sotirios Argyroudis:** Writing – review & editing, Visualization, Validation, Supervision, Methodology, Conceptualization. **Stergios-Aristoteles Mitoulis:** Writing – review & editing, Supervision, Methodology, Conceptualization.

## Declaration of competing interest

The authors declare that they have no known competing financial interests or personal relationships that could have appeared to influence the work reported in this paper.

## Acknowledgments

The first author appreciates the support from the National Natural Science Foundation of China (52478410, W2411044, and 52408435), the National Key Research and Development Program of China (2022YFC3800905), Young Elite Scientists Sponsorship Program by CAST (2023QNRC001), and the Fundamental Research Funds for the Central Universities.

Dr. Stergios-Aristoteles Mitoulis and Dr. Sotirios Argyroudis acknowledge funding from the UK Research and Innovation (UKRI) under the UK government's Horizon Europe funding guarantee (EP/Y003586/1, EP/X037665/1). This is the funding guarantee for the European Union's HORIZON-MSCA-2021-SE-01 (101086413) "ReCharged—Climate-Aware Resilience for Sustainable Critical and Interdependent Infrastructure Systems Enhanced by Emerging Digital Technologies."

The authors would like to acknowledge the invaluable support of the 33 experts for their insightful input and participation in the survey.

## Appendix A. Supplementary data

Supplementary data to this article can be found online at https://doi.org/10.1016/j.eng.2025.06.028.

## References

[1] Sterling RL. Advances in underground construction help provide quality of life for modern societies. Engineering 2017;3(6):780–1.
[2] Zhao Y, Li PF. A Statistical analysis of China's traffic tunnel development data. Engineering 2018;4(1):3–5.
[3] Meguid MA, Saada O, Nunes MA, Mattar J. Physical modeling of tunnels in soft ground: a review. Tunn Undergr Space Technol 2008;23(2):185–98.
[4] Qian QH. Present state, problems and development trends of urban underground space in China. Tunn Undergr Space Technol 2016;55:280–9.
[5] Mandal T, Rao KR, Tiwari G. Evacuation of metro stations: a review. Tunn Undergr Space Technol 2023;140:105304.
[6] Koks EE, Rozenberg J, Zorn C, Tariverdi M, Vousdoukas M, Fraser SA, et al. A global multi-hazard risk analysis of road and railway infrastructure assets. Nat Commun 2019;10(1):2677.
[7] Pescaroli G, Alexander D. Critical infrastructure, panarchies and the vulnerability paths of cascading disasters. Nat Hazards 2016;82(1):175–92.
[8] Padgett JE, Panakkal P, González-Dueñas C. Infrastructure impacts and vulnerability to coastal flood events. In: Brody S, Lee Y, Kothuis B, editors. Coastal flood risk reduction. Amsterdam: Elsevier; 2022. p. 151–65.

[9] Padgett J, DesRoches R, Nielson B, Yashinsky M, Kwon OS, Burdette N, et al. Bridge damage and repair costs from Hurricane Katrina. J Bridge Eng 2008;13(1):6–14.
[10] Ozcan AK, Gokceoglu C. Statistical assessment of geological and geomorphological factors on building damages caused by the February 6, 2023 earthquakes in the Amanos region of Türkiye. Nat Hazards Rev 2025;26(1):04024052.
[11] Galasso C, Opabola EA. The 2023 Kahramanmaraş earthquake sequence: finding a path to a more resilient, sustainable, and equitable society. Commun Eng 2024;3(1):24.
[12] Apostolaki S, Karahan S, Riga E, Tsinidis G, Gokceoglu C, Pitilakis K. Seismic performance of tunnels and verification of available seismic risk models for the 2023 Kahramanmaraş earthquakes. Tunn Undergr Space Technol 2025;156:106185.
[13] Wang WL, Wang TT, Su JJ, Lin CH, Seng CR, Huang TH. Assessment of damage in mountain tunnels due to the Taiwan Chi-Chi earthquake. Tunn Undergr Space Technol 2001;16(3):133–50.
[14] Wang TT, Kwok OLA, Jeng FS. Seismic response of tunnels revealed in two decades following the 1999 Chi-Chi earthquake (Mw 7.6) in Taiwan: a review. Eng Geol 2021;287:106090.
[15] Callisto L, Ricci C. Interpretation and back-analysis of the damage observed in a deep tunnel after the 2016 Norcia earthquake in Italy. Tunn Undergr Space Technol 2019;89:238–48.
[16] Carter MR, Howard MP, Owens N, Register D, Kennedy J, Pecheux K, et al. Effects of catastrophic events on transportation system management and operations. Report. Washington, DC: US Department of Transportation; 2002.
[17] Li YZ, Ingason H. Overview of research on fire safety in underground road and railway tunnels. Tunn Undergr Space Technol 2018;81:568–89.
[18] Hong H. The progress and controlling situation of Daegu subway fire disaster. In: Proceedings of the Sixth Asia–Oceania Symposium on Fire Science and Technology, 2004 Mar 17–20, Daegu, Korea. Seoul: Korean Institute of Fire Science & Engineering; 2004. p. 28–46.
[19] Sun ML, Liang HW, Zhu YQ, Gao XQ, Liu H, Zhu ZG. Deformation and failure mode analysis of the tunnel structure based on the tunnel-related landslides cases. Front Earth Sci 2022;10:906884.
[20] Sosa EM, Thompson GJ, Barbero EJ. Testing of full-scale inflatable plug for flood mitigation in tunnels. Transp Res Rec 2014;2407(1):59–67.
[21] Yang H, Zhao L, Chen J. Metro system inundation in Zhengzhou, Henan Province, China. Sustainability 2022;14(15):9292.
[22] Cheng R, Chen W, Hao H, Li J. A state-of-the-art review of road tunnel subjected to blast loads. Tunn Undergr Space Technol 2021;112:103911.
[23] Colglazier W. Sustainable development agenda: 2030. Science 2015;349(6252):1048–50.
[24] Opabola EA, Galasso C. Informing disaster-risk management policies for education infrastructure using scenario-based recovery analyses. Nat Commun 2024;15(1):325.
[25] Linkov I, Bridges T, Creutzig F, Decker J, Fox-Lent C, Kröger W, et al. Changing the resilience paradigm. Nat Clim Chang 2014;4(6):407–9.
[26] Achillopoulou DV, Mitoulis SA, Argyroudis SA, Wang Y. Monitoring of transport infrastructure exposed to multiple hazards: a roadmap for building resilience. Sci Total Environ 2020;746:141001.
[27] Blockley D, Agarwal J, Godfrey P. Infrastructure resilience for high-impact low-chance risks. Proc Inst Civ Eng Civ Eng 2012;165(6):13–9.
[28] Cimellaro GP, Reinhorn AM, Bruneau M. Framework for analytical quantification of disaster resilience. Eng Struct 2010;32(11):3639–49.
[29] Psyrras NK, Sextos AG. Safety of buried steel natural gas pipelines under earthquake-induced ground shaking: a review. Soil Dyn Earthq Eng 2018;106:254–77.
[30] Kopiika N, Mitoulis SA, Ninic J. Resilience framework for aged bridges subjected to human-induced hazard-case study in Ukraine. In: Proceedings of the International Conference of Coordinating Engineering for Sustainability and Resilience, 2024 May 29–31, Timișoara, Romania. Cham: Springer Nature; 2024. p. 50–62.
[31] Cimellaro GP, Renschler C, Reinhorn AM, Arendt L. PEOPLES: a framework for evaluating resilience. J Struct Eng 2016;142(10):04016063.
[32] Bruneau M, Chang SE, Eguchi RT, Lee GC, O'Rourke TD, Reinhorn AM, et al. A framework to quantitatively assess and enhance the seismic resilience of communities. Earthq Spectra 2003;19(4):733–52.
[33] Argyroudis SA, Mitoulis SA, Hofer L, Zanini MA, Tubaldi E, Frangopol DM. Resilience assessment framework for critical infrastructure in a multi-hazard environment: case study on transport assets. Sci Total Environ 2020;714:136854.
[34] Mitoulis SA, Argyroudis SA, Loli M, Imam B. Restoration models for quantifying flood resilience of bridges. Eng Struct 2021;238:112180.
[35] Argyroudis SA. Resilience metrics for transport networks: a review and practical examples for bridges. Proc Inst Civ Eng-Bridge Eng 2022;175(3):179–92.
[36] Chen X, Shen J, Bao X, Wu X, Tang W, Cui H. A review of seismic resilience of shield tunnels. Tunn Undergr Space Technol 2023;136:105075.
[37] Makhoul N, Roohi M, van de Lindt JW, Sousa H, Santos LO, Argyroudis S, et al. Seismic resilience of interdependent built environment for integrating structural health monitoring and emerging technologies in decision-making. Struct Eng Int 2024;34(1):19–33.
[38] Orlacchio M, Chioccarelli E, Iervolino I. State-dependent fragility functions for Italian building classes. Soil Dyn Earthq Eng 2024;182:108685.
[39] Rincon R, Padgett JE. Fragility modeling practices and their implications on risk and resilience analysis: from the structure to the network scale. Earthq Spectra 2024;40(1):647–73.
[40] Argyroudis SA, Mitoulis SA, Winter MG, Kaynia AM. Fragility of transport assets exposed to multiple hazards: state-of-the-art review toward infrastructural resilience. Reliab Eng Syst Saf 2019;191:106567.
[41] Silva V, Akkar S, Baker J, Bazzurro P, Castro JM, Crowley H, et al. Current challenges and future trends in analytical fragility and vulnerability modeling. Earthq Spectra 2019;35(4):1927–52.
[42] Long X, Ma Y, Miao Y, Ye L, Zhou W. Longitudinal seismic fragility analysis of long tunnels under multiple support excitation. Soil Dyn Earthq Eng 2023;164:107608.
[43] Stefanidou SP, Kappos AJ. Bridge-specific fragility analysis: when is it really necessary? Bull Earthq Eng 2019;17(4):2245–80.
[44] Wilson G, Wilson TM, Deligne NI, Blake DM, Cole JW. Framework for developing volcanic fragility and vulnerability functions for critical infrastructure. J Appl Volcanol 2017;6(1):14.
[45] Dong Z, Kuo C, Yin J, Wen S, Liu G, Gou Y. Examination of longitudinal seismic vulnerability of shield tunnels utilizing incremental dynamic analysis. Front Earth Sci 2021;9:779879.
[46] Huang ZK, Pitilakis K, Tsinidis G, Argyroudis S, Zhang DM. Seismic vulnerability of circular tunnels in soft soil deposits: the case of Shanghai metropolitan system. Tunn Undergr Space Technol 2020;98:103341.
[47] Nguyen DD, Park D, Shamsher S, Nguyen VQ, Lee TH. Seismic vulnerability assessment of rectangular cut-and-cover subway tunnels. Tunn Undergr Space Technol 2019;86:247–61.
[48] Kazemi F, Asgarkhani N, Jankowski R. Machine learning-based seismic fragility and seismic vulnerability assessment of reinforced concrete structures. Soil Dyn Earthq Eng 2023;166:107761.
[49] Amorosi A, Boldini D. Numerical modelling of the transverse dynamic behaviour of circular tunnels in clayey soils. Soil Dyn Earthq Eng 2009;29(6):1059–72.
[50] Cabangon LT, Elia G, Rouainia M. Modelling the transverse behaviour of circular tunnels in structured clayey soils during earthquakes. Acta Geotech 2019;14(1):163–78.
[51] Li P, Song EX. Three-dimensional numerical analysis for the longitudinal seismic response of tunnels under an asynchronous wave input. Comput Geotech 2015;63:229–43.
[52] Liu C, Peng Z, Cui J, Huang X, Li Y, Chen W. Development of crack and damage in shield tunnel lining under seismic loading: refined 3D finite element modeling and analyses. Thin-walled Struct 2023;185:110647.
[53] Tsinidis G. Response of urban single and twin circular tunnels subjected to transversal ground seismic shaking. Tunn Undergr Space Technol 2018;76:177–93.
[54] Duan Y, Zhao M, Huang J, Li H, Du X. Analytical solution for circular tunnel under obliquely incident *P* waves considering different contact conditions. Shock Vib 2021;2021(1):1–23.
[55] Li H, Zhao M, Huang J, Lia W, Zhao X, Du X. Simplified analytical solutions for deep tunnels subjected to vertically incident shear wave with arbitrary vibration direction. Soil Dyn Earthq Eng 2022;156:107245.
[56] Li H, Zhou N, Huang J, Zhao M, Liao W, Zhao X, et al. Analytical solution of longitudinal seismic response of circular tunnel across soil–rock stratum based on improved elastic foundation beam model. Comput Geotech 2023;159:105383.
[57] Zhao W, Gao H, Chen W, Xie P. Analytical study on seismic response of subsea tunnels in a multi-layered seabed subjected to *P*- and SV-waves. Tunn Undergr Space Technol 2023;134:105015.
[58] Chen Z, Bian M. Dynamic centrifuge test and numerical modelling of the seismic response of the tunnel in cohesive soil foundation. Buildings 2022;12(3):337.
[59] Moghadam MR, Baziar MH. Seismic ground motion amplification pattern induced by a subway tunnel: shaking table testing and numerical simulation. Soil Dyn Earthq Eng 2016;83:81–97.
[60] Zhang S, Yuan Y, Yang Y, Li C, Yu H. Experimental investigation of seismic performance of segmental tunnel with secondary lining under strong earthquake. Structures 2024;60:105833.
[61] Hu H, Qiu WG. Study on earthquake damage characteristic on mountain tunnel and analysis. Appl Mech Mater 2011;94:1078–81.
[62] Shen Y, Gao B, Yang X, Tao S. Seismic damage mechanism and dynamic deformation characteristic analysis of mountain tunnel after Wenchuan earthquake. Eng Geol 2014;180:85–98.
[63] Huang Z. Resilience evaluation of shallow circular tunnels subjected to earthquakes using fragility functions. Appl Sci 2022;12(9):4728.
[64] Huang Z, Zhang D, Pitilakis K, Tsinidis G, Huang H, Zhang D, et al. Resilience assessment of tunnels: framework and application for tunnels in alluvial deposits exposed to seismic hazard. Soil Dyn Earthq Eng 2022;162:107456.
[65] Xu C, Hu H, Wang H. A theoretical study on the resilience evaluation method of operational road tunnel systems. Appl Sci 2023;13(24):13279.
[66] Anwar GA, Dong Y. Seismic resilience of retrofitted RC buildings. Earthq Eng Eng Vib 2020;19(3):561–71.
[67] Biondini F, Camnasio E, Titi A. Seismic resilience of concrete structures under corrosion. Earthq Eng Struct Dyn 2015;44(14):2445–66.
[68] Shang Q, Wang T, Li J. A quantitative framework to evaluate the seismic resilience of hospital systems. J Earthq Eng 2022;26(7):3364–88.
[69] Cimellaro GP, Reinhorn AM, Bruneau M. Seismic resilience of a hospital system. Struct Infrastruct Eng 2010;6(1–2):127–44.

[70] Zhou Y, Wu H, Gu AQ. Earthquake engineering: from earthquake resistance, energy dissipation, and isolation, to resilience. Eng Mech 2019;36(6):1–12. Chinese.
[71] Decò A, Bocchini P, Frangopol DM. A probabilistic approach for the prediction of seismic resilience of bridges. Earthq Eng Struct Dyn 2013;42(10):1469–87.
[72] Misra S, Padgett JE, Barbosa AR, Webb BM. An expert opinion survey on post-hazard restoration of roadways and bridges: data and key insights. Earthq Spectra 2020;36(2):983–1004.
[73] Gidaris I, Padgett JE, Barbosa AR, Chen S, Cox D, Webb B, et al. Multiple-hazard fragility and restoration models of highway bridges for regional risk and resilience assessment in the United States: state-of-the-art review. J Struct Eng 2017;143(3):04016188.
[74] Bocchini P, Deco A, Frangopol DM. Probabilistic functionality recovery model for resilience analysis. In: Proceedings of the Sixth International Bridge Maintenance, Safety, Management, Resilience and Sustainability (IABMAS) Conference, 2012 Jul 8–12, Stresa, Italy. London: CRC Press; 2012. p. 1920–7.
[75] Bocchini P, Frangopol DM. Optimal resilience-and cost-based postdisaster intervention prioritization for bridges along a highway segment. J Bridge Eng 2012;17(1):117–29.
[76] Padgett JE, DesRoches R. Bridge functionality relationships for improved seismic risk assessment of transportation networks. Earthq Spectra 2007;23(1):115–30.
[77] Federal Emergency Management Agency (FEMA), National Institute of Building Sciences (NIBS). Hazus 4.2 SP3: Hazus earthquake model technical manual. Washington, DC: FEMA-NIBS; 2020.
[78] Tubaldi E, Macorini L, Izzuddin BA, Manes C, Laio F. A framework for probabilistic assessment of clear-water scour around bridge piers. Struct Saf 2017;69:11–22.
[79] GB50157–2013: Code for design of metro. Chinese standard. Beijing: Ministry of Housing and Urban-Rural Development of the People's Republic of China; 2013. Chinese.
[80] Tsinidis G, Karatzetzou A, Stefanidou S. On the effects of salient parameters for an efficient assessment of seismic response and fragility of circular tunnels in clayey deposits. Soil Dyn Earthq Eng 2024;178:108490.
[81] Cabangon LT, Elia G, Rouainia M, Keawsawasvong S, Ornthammarath T. Seismic vulnerability of shallow tunnels subjected to far-field long-period ground motions. Soil Dyn Earthq Eng 2024;176:108313.
[82] Mair RJ. Tunnelling and geotechnics: new horizons. Geotechnique 2008;58(9):695–736.
[83] Pinto F, Whittle AJ. Ground movements due to shallow tunnels in soft ground. I: analytical solutions. J Geotech Geoenviron Eng 2014;140(4):04013040.
[84] Huang HW, Zhang DM. Resilience analysis of shield tunnel lining under extreme surcharge: characterization and field application. Tunn Undergr Space Technol 2016;51:301–12.
[85] British Tunnelling Society; Institution of Civil Engineers. Tunnel lining design guide. London: Thomas Telford Publishing; 2004.
[86] DGJ08-11-99: Shanghai foundation design code. Chinese standard. Shanghai: Shanghai Municipal Commission of Housing and Urban-Rural Development; 2013. Chinese.
[87] Argyroudis SA, Pitilakis KD. Seismic fragility curves of shallow tunnels in alluvial deposits. Soil Dyn Earthq Eng 2012;35:1–12.
[88] Le TS, Huh J, Park JH. Earthquake fragility assessment of the underground tunnel using an efficient SSI analysis approach. Z Angew Math Phys 2014;2(12):1073.
[89] Jamshidi Avanaki M, Hoseini A, Vahdani S, de Santos C, de la Fuente A. Seismic fragility curves for vulnerability assessment of steel fiber reinforced concrete segmental tunnel linings. Tunn Undergr Space Technol 2018;78:259–74.
[90] Argyroudis S, Tsinidis G, Gatti F, Pitilakis K. Effects of SSI and lining corrosion on the seismic vulnerability of shallow circular tunnels. Soil Dyn Earthq Eng 2017;98:244–56.
[91] Huang G, Qiu W, Zhang J. Modelling seismic fragility of a rock mountain tunnel based on support vector machine. Soil Dyn Earthq Eng 2017;102:160–71.
[92] Reddy AD, Singh A. A new post-seismic damage classification for rock tunnels based on analysis of 26 global earthquakes. Geotech Geol Eng 2024;42(8):6997–7023.
[93] Reddy AD, Singh A. A simplistic method for assessing seismic damage in rock tunnels before earthquake: part 1: damage prediction and validation using seismic damage classification of tunnels. Rock Mech Rock Eng 2024;57(8):11001–32.
[94] Zhang D, Zhai W, Huang H, Chapman D. Robust retrofitting design for rehabilitation of segmental tunnel linings: using the example of steel plates. Tunn Undergr Space Technol 2019;83:231–42.
[95] Zhang D, Liu Z, Wang R, Zhang D. Influence of grouting on rehabilitation of an over-deformed operating shield tunnel lining in soft clay. Acta Geotech 2019;14(4):1227–47.
[96] Kunita M, Takemata R, Iai Y. Restoration of a tunnel damaged by earthquake. Tunn Undergr Space Technol 1994;9(4):439–48.
[97] Jiang Y, Wang L, Zhang B, Dai X, Ye J, Sun B, et al. Tunnel lining detection and retrofitting. Autom Construct 2023;152:104881.
[98] Zhang DM, Zhang DM, Soga K, Huang HW, Wang F. Rehabilitation of overdeformed metro tunnel in Shanghai by multiple repair measures. J Geotech Geoenviron Eng 2019;145(11):04019101.
[99] Tang Y, Zhu Z, Ba Z, Lee VW, Gong W. Running safety assessment of trains considering post-earthquake damage state of bridge–track system. Eng Struct 2023;287:116187.
[100] Wang H, Xiao J, Li S, Zhai C. Resilience assessment and optimization method of city road network in the post-earthquake emergency period. Earthq Eng Eng Vib 2024;23(5):765–79.
[101] Wu S, Wu Z, Zhang C. Rock burst prediction probability model based on case analysis. Tunn Undergr Space Technol 2019;93:103069.
[102] Karamlou A, Bocchini P. Functionality-fragility surfaces. Earthq Eng Struct Dyn 2017;46(10):1687–709.
[103] El Haj AK, Soubra AH, Fajoui J. Probabilistic analysis of an offshore monopile foundation taking into account the soil spatial variability. Comput Geotech 2019;106:205–16.
[104] Chen Y, Liu W, Ai D, Zhu H, Du Y. Probabilistic reliability assessment method for max ground settlement prediction of subway tunnel under uncertain construction information. Comput Geotech 2025;177:106805.
[105] Zhang H, Wu Y, Yang S. Probabilistic analysis of tunnel convergence in spatially variable soil based on Gaussian process regression. Eng Appl Artif Intell 2024;131:107840.
[106] Zou Y, Zhang Y, Liu H, Liu H, Miao Y. Performance-based seismic assessment of shield tunnels by incorporating a nonlinear pseudostatic analysis approach for the soil–tunnel interaction. Tunn Undergr Space Technol 2021;114:103981.
[107] Argyroudis SA, Nasiopoulos G, Mantadakis N, Mitoulis SA. Cost-based resilience assessment of bridges subjected to earthquakes. Int J Disaster Resil Built Environ 2021;12(2):209–22.
[108] Pang Y, Wang X. Cloud–IDA–MSA conversion of fragility curves for efficient and high-fidelity resilience assessment. J Struct Eng 2021;147(5):04021049.
[109] Zhou L, Alam MS, Dong Y, Feng R. Seismic resilience assessment of extended pile shaft supported coastal bridges considering scour and uniform corrosion effects. Eng Struct 2024;304:117643.
[110] Gonzalez C, Niño M, Jaimes MA. Event-based assessment of seismic resilience in Mexican school buildings. Bull Earthq Eng 2020;18(14):6313–36.
[111] Reed DA, Kapur KC, Christie RD. Methodology for assessing the resilience of networked infrastructure. IEEE Syst J 2009;3(2):174–80.
[112] Samadian D, Ghafory-Ashtiany M, Naderpour H, Eghbali M. Seismic resilience evaluation based on vulnerability curves for existing and retrofitted typical RC school buildings. Soil Dyn Earthq Eng 2019;127:105844.
[113] Trump BD, Mitoulis S, Argyroudis S, Kiker G, Palma-Oliveira J, Horton R, et al. Threat-agnostic resilience: Framing and applications. Int J Disaster Risk Reduct 2025;124:105535.
[114] Sun J, Bathgate K, Zhang Z. Bayesian network-based resilience assessment of interdependent infrastructure systems under optimal resource allocation strategies. Resil Cities Struct 2024;3(2):46–56.
[115] Roohi M, Ghasemi S, Sediek O, Jeon H, van de Lindt JW, Shields M, et al. Multi-disciplinary seismic resilience modeling for developing mitigation policies and recovery planning. Resil Cities Struct 2024;3(2):66–84.
[116] Gogate NG, Shelake AG, Band P. Selection of most significant risk factors for Indian tunnel projects: an integrated fuzzy-based MCDM approach. Int J Constr Manag 2024;24(2):161–76.
[117] Han K, Zhang D, Chen X, Su D, Ju JWW, Lin XT, et al. A resilience assessment framework for existing underground structures under adjacent construction disturbance. Tunn Undergr Space Technol 2023;141:105339.
[118] Coussement K, Benoit DF, Antioco M. A Bayesian approach for incorporating expert opinions into decision support systems: a case study of online consumer-satisfaction detection. Decis Support Syst 2015;79:24–32.
[119] Fan M, Liu Y, Liu K, Zhang C, Li Y, Liu X, et al. Constructing a resilience assessment index system for tuberculosis healthcare services under public health emergencies: a modified Delphi study. Risk Manag Healthc Policy 2025;18:1057–67.